



# Peptides-tethered vascular grafts enable blood vessel regeneration via endogenous cell recruitment and neovascularization

Yifan Wu<sup>a,b,1</sup>, Lili Song<sup>a</sup>, Muhammad Shafiq<sup>c,d,\*,1</sup>, Hiroyuki Ijima<sup>c</sup>, Soo Hyun Kim<sup>e,f</sup>,  
Ran Wei<sup>a</sup>, Deling Kong<sup>b</sup>, Xiumei Mo<sup>d,\*\*</sup>, Kai Wang<sup>b,\*\*\*</sup>

<sup>a</sup> College of Life Sciences, Tiangong University, Tianjin, 300387, China

<sup>b</sup> College of Life Sciences, Key Laboratory of Bioactive Materials (Ministry of Education), State Key Laboratory of Medicinal Chemical Biology, Nankai University, Tianjin, 300071, China

<sup>c</sup> Department of Chemical Engineering, Faculty of Engineering, Graduate School, Kyushu University, Fukuoka, 819-0395, Japan

<sup>d</sup> State Key Laboratory for Modification of Chemical Fibers and Polymer Materials, Shanghai Engineering Research Center of Nano-Biomaterials and Regenerative Medicine, College of Biological Science and Medical Engineering, Donghua University, Shanghai, 201620, China

<sup>e</sup> Center for Biomaterials, Biomedical Research Institute, Korea Institute of Science and Technology, Seoul, Republic of Korea

<sup>f</sup> Korea Institute of Science and Technology Europe, Saarbrücken, Germany

## ARTICLE INFO

Handling Editor: Dr Hao Wang

### Keywords:

Vascular grafts  
Electrospinning  
Polymer modification  
Peptide  
SDF-1 $\alpha$   
Stem cell recruitment  
*In situ* tissue regeneration

## ABSTRACT

Cardiovascular injuries cause huge morbidity and mortality worldwide. Arterial reconstructions are generally performed either by using native grafts or synthetic grafts, both of which are limited by several complications. Synthetic biodegradable polymers offer a promising platform, which may also be modified to foster *in situ* tissue regeneration through the recruitment of host cells. Vascular endothelial growth factor (VEGF) promotes endothelialization and neovascularization in vascular grafts, however, an overdose of VEGF may induce tumor-like vasculature, which requires alternative strategies. The objective of this study was to exploit prominin-1-derived VEGF-binding peptide (BP) to improve neovascularization and endothelialization, while stromal cell-derived factor 1-alpha (SDF-1 $\alpha$ ) peptide to encourage endogenous stem/progenitor cells mobilization and complement BP-mediated vascular remodeling. The BP and SDF-1 $\alpha$  peptides were covalently conjugated with low molecular weight poly ( $\epsilon$ -caprolactone) (LPCL) to afford LPCL-BP and LPCL-SDF-1 $\alpha$ , respectively. Chemical analysis revealed successful modification of LPCL with peptides, which also displayed good cytocompatibility *in vitro* once blended along with high molecular weight PCL (HPCL). The bioactivated vascular grafts were fabricated by blending LPCL-BP, LPCL-SDF-1 $\alpha$  or dual peptide-polymer conjugates with HPCL. The *in vivo* tests of vascular grafts through rat abdominal aorta implantation model revealed that, compared with HPCL grafts, the dual peptides modified grafts exhibited superior patency and tissue regeneration at 4-week post-implantation, including stem cell recruitment, rapid endothelialization and functional SMC layer formation. Taken together, these results may have implications for the *in situ* regeneration of artificial blood vessels through the orchestration of host's responses and endogenous cell recruitment.

## 1. Introduction

Cardiovascular injuries cause huge morbidity and mortality worldwide [1]. Ideal replacements for injured blood vessels include grafting of native arteries, such as the saphenous vein. While being a gold-standard, these grafts are limited owing to the acute shortage of appropriate

donors as well as morbidity risks [2]. Similarly, tissue engineered vascular grafts are hampered by the excessive *ex vivo* cell manipulations, which obviously require more time for cell culture in bioreactors under static or dynamic conditions [3]. To circumvent these limitations, polymers, including expanded polytetrafluoroethylene (ePTFE) and poly (ethylene terephthalate) (PET, Dacron) have been used to fabricate

\* Corresponding author. Department of Chemical Engineering, Faculty of Engineering, Graduate School, Kyushu University, Fukuoka, 819-0385, Japan.

\*\* Corresponding author.

\*\*\* Corresponding author.

E-mail addresses: [shafiqdr786@yahoo.com](mailto:shafiqdr786@yahoo.com) (M. Shafiq), [xmm@dhu.edu.cn](mailto:xmm@dhu.edu.cn) (X. Mo), [013053@nankai.edu.cn](mailto:013053@nankai.edu.cn) (K. Wang).

<sup>1</sup> These authors contributed equally to this work.

artificial blood vessels, which are now being clinically used for large diameter vascular grafts ( $ID \geq 6$  mm). However, these grafts exhibit poor short- and long-term patency, especially when transplanted in small-caliber blood vessels ( $ID < 6$  mm) [4,5]. Recently, biodegradable polymers based grafts have been studied by using different types of synthetic biodegradable polymers, such as polycaprolactone (PCL), poly(L-lactide-co- $\epsilon$ -caprolactone) (PLCL) and poly(glycerol sebacate) (PGS) [6–9]. However, the hydrophobicity and poor cell affinity of these polymers limit their use. This necessitates polymer modification to not only increase cell infiltration but to also modulate host responses for vascular remodeling [10,11]. Consequently, bioactive cues are either encapsulated into vascular grafts during fabrication or immobilized onto vascular graft surface post-fabrication [12]. Bulk modification of polymers followed by graft fabrication is an alternative approach for the functionalization of vascular grafts.

*In situ* tissue regeneration through the recruitment of host stem/progenitor cells holds great promise [13,14]. Exogenously cell-seeded grafts may induce vascular remodeling either by differentiating into targeted vascular cell types or by paracrine mechanisms [15]. However, limitations associated with the exogenous cells, such as extensive *ex vivo* cell manipulations, poor retention, limited engraftment *in vivo*, and antigenicity risks may hamper their utilization [16,17]. Alternatively, cell-free vascular grafts rely on the recruitment of endogenous stem/progenitor cells from the host, which may avoid the aforementioned limitations, but the limited number of host stem/progenitor cells may be insufficient for *in situ* tissue regeneration. A multitude of bioactive cues, including SDF-1 $\alpha$ , neuropeptide substance P (SP), and VEGF have been shown to induce *in situ* tissue vascular regeneration by inducing the mobilization and recruitment of endogenous stem/progenitor cells as well as their differentiation into vascular cell types [18–20].

The VEGF is a potent vasculogenic and angiogenic molecule, which has been shown to promote endothelialization and neovascularization by promoting the viability, proliferation and migration of ECs. The VEGF-loaded vascular grafts were shown to be patent owing to endogenous recruitment of CD31-, CD34-, and vWF-positive cells [20–22]. Besides, VEGF may induce nitric oxide (NO) production and improve vascular permeability [20]. Nonetheless, VEGF alone may be insufficient to induce *in situ* vascular regeneration and an overdose of VEGF may induce tumor-like vasculature [22]. Alternative strategies could be opted to abrogate VEGF shortcomings, such as the use of short amino-acid sequences with similar biological activity to the VEGF [23, 24]. Adini et al. exploited prominin-1-derived VEGF-binding peptide (BP) consisting of 12-amino acids, which enhanced neovascularization in a corneal injury model. Besides, BP improved outcome in different disease models, such as hind-limb ischemia, choroidal neovascularization and MI model and enhanced VEGF binding to its receptors, including VEGF-R1 and neuropilin-1 [25,26]. The recruitment of VEGF by BP at the implantation site may have multiple benefits for arterial grafts, such as rapid endothelialization, vascular remodeling into the graft wall, and implant/host tissue anastomosis [24]. Moreover, the VEGF may also induce the differentiation of stem/progenitor cells into vascular cell types to further promote endothelialization and vascular remodeling [27,28]. Nonetheless, a bolus injection or simple blending of BP into scaffolds may not be sufficient to realize VEGF-mediated therapeutic benefits [22,24,29]. Alternative cues are therefore needed to support VEGF-driven endothelialization and successful regeneration of SMCs.

The VEGF used along with basic fibroblast growth factor (bFGF) and SDF-1 $\alpha$  was shown to induce re-endothelialization and vascular remodeling [22]. These effects were superior when VEGF was used alone. It is noteworthy to mention here that while different types of cytokines/chemokines can induce the mobilization and recruitment of endogenous stem/progenitor cells, SDF-1 $\alpha$  is a potent chemoattractant of EPCs as well as smooth muscle progenitor cells (SMPCs), which has been widely explored for vascular tissue engineering [30]. However, SDF-1 $\alpha$  exhibits large molecular weight, which cannot be easily

synthesized. Meanwhile, SDF-1 $\alpha$  can be easily degraded by matrix metalloproteinases (MMPs), which may further limit its application prospect [31]. Alternatively, the SDF-1 $\alpha$  peptide has short amino acid sequences, which can replicate the function of full-length proteins, can be easily synthesized and resisted to MMPs protease [31]. SDF-1 $\alpha$  peptide encapsulating grafts were shown to promote endothelium regeneration as well as stem/progenitor cell recruitment *in vivo* [19]. However, the rapid release of the encapsulated SDF-1 $\alpha$  may be insufficient to promote vascular remodeling [32,33]. The SDF-1 $\alpha$  derived peptide was previously conjugated with star-shaped PLCL copolymers as well as encapsulated into PCL-based grafts and shown to promote endogenous cell recruitment and tissue regeneration [32].

Biomolecules can be incorporated into scaffolds by different methods, such as blending with polymers during electrospinning, surface modification through physisorption, and covalent immobilization post-fabrication. However, it may require chemical modification of surface via aminolysis, hydrolysis, or chemical grafting, thereby adversely affecting the bioactivity of biological cues as well as topography and morphology of scaffold structure [34,35]. Alternatively, bulk-modification may avoid these limitations, it involves the tethering of bioactive cues, such as peptide conjugated with polymers before the fabrication of scaffolds. By using bulk conjugation method, a myriad of bioactive cues, such as SP, mesenchymal stem cell (MSC)-affinity peptide, and SDF-1 $\alpha$  peptide have been conjugated with PLCL copolymers [18,32]. These peptides-tethered polymers can be fabricated into different shapes and structures, such as nanofibers, scaffolds and nanoparticles, as needed for tissue engineering applications [36]. Therefore, bulk modified polymeric biomaterials may exhibit great potential than that of the other modification methods.

Consequently, the overarching goal of this research was to confer bioactivity to PCL-based small-diameter vascular grafts by simultaneously harnessing the beneficial effects of BP and SDF-1 $\alpha$  peptide. While the SDF-1 $\alpha$  peptide can recruit the host vascular progenitor cells (VPCs), the BP can *in situ* capture VEGF at the injury site to further expedite endothelialization and SMCs regeneration. BP and SDF-1 $\alpha$  peptide were first conjugated to LPCL and the bioactive peptide-polymer conjugates were next blended along with the HPCL to afford small-diameter vascular grafts. Different types of *in vitro* and *in vivo* experiments delineated the superiority of bioactivated vascular grafts than that of the HPCL grafts. Taken together, our approach of simultaneously exploiting stem cell inducing/recruiting factors and angiogenic factors may hold great promise for vascular regeneration applications.

## 2. Materials and methods

### 2.1. Materials

PCL ( $M_n = 14000$  Da,  $M_w = 80000$  Da) pellets were obtained from Sigma-Aldrich (St. Louis, MO, USA). SDF-1 $\alpha$  peptide (CGSKPVVLSYR) and prominin-1-derived VEGF-binding peptide (PR1P, herein named as BP, CGDRVQRQTTTVVA) containing an extra cysteine and glycine residues were acquired from QiangYao Biotech Co. Ltd. (Shanghai, China) with a purity of  $\geq 95\%$ . Other chemical reagents were bought from Tianjin Chemical Reagent Company (Tianjin, China). For *in vitro* studies, cell culture reagents were acquired from Thermo Fisher Scientific (Waltham, MA, USA). CCK8 reagent was purchased from Biosharp (Hefei, China). Live & Dead cell staining kit was obtained from Solarbio (Beijing, China). For *in vivo* studies, primary antibodies (CD68, ab125212; iNOS, ab15323; CD206, ab64693; CD31, ab64543 and  $\alpha$ -SMA, ab7817) were purchased from Abcam (Cambridge, UK). Other primary Sca-1 antibody (AB4336) and MYH11 antibody (sc-6956) were bought from Merck Millipore (Burlington, MA, USA) and Santa Cruz Biotechnology (Santa Cruz, CA, USA), respectively. The secondary antibodies were obtained from Invitrogen (Carlsbad, CA, USA). The staining kits for Safranin O and Masson's Trichrome staining were acquired from Solarbio (Beijing, China). Verhoeff van Gieson (VVG) and

Haematoxylin and Eosin (H&E) staining kits were purchased from Leagene (Beijing, China). The DAPI was purchased from Southern Biotech Company (Birmingham, AL, USA).

## 2.2. Synthesis and characterization of peptide-polymer conjugates

### 2.2.1. Synthesis of peptide-polymer conjugates

It is noteworthy to mention here that we conjugated BP or SDF-1 $\alpha$  peptide with LPCL ( $M_n = 14$  kDa) due to the ease of conjugation of peptides at both ends of LPCL as well as more numbers of functional groups than that of the HPCL. The LPCL of this particular molecular weight was used to ensure the insolubility of peptide-polymer conjugates in water [36,37]. Briefly, the hydroxyl (-OH) groups at the both ends of LPCL were first modified with *p*-maleimidophenyl isocyanate (PMPI) and were then reacted with the cysteine-tagged peptides through Michael type addition. In detail, the LPCL was vacuum dried for up to 6 h to remove moisture and dissolved in N-Methyl-2-pyrrolidone (NMP) under inert environment. Once the homogenous solution was obtained, PMPI was dissolved in 2 mL of NMP at 8-fold molar excess than that of the LPCL, added drop-wise into LPCL solution, and reacted overnight. The solution was precipitated in cooled diethyl ether and vacuum dried for up to 3 days. The LPCL-PMPI was next dissolved in NMP under inert environment. The BP or SDF-1 $\alpha$  peptide was dissolved in 1 mL of anhydrous DMSO and drop-wise added into LPCL-PMPI solution at 4-fold molar excess and reacted for up to 24 h. The LPCL-BP and LPCL-SDF-1 $\alpha$  were precipitated in cooled diethyl ether, vacuum dried, and stored at  $-20$  °C.

### 2.2.2. Characterization of peptide-polymer conjugates

The structural analysis of LPCL-BP and LPCL-SDF-1 $\alpha$  was tested using Fourier transform infrared spectroscopy (FTIR, Nicolet-760, Madison, WI) and X-ray photoelectron spectroscopy (XPS, Kratos Analytical, Manchester, UK). Thermogravimetric analysis was carried out in nitrogen ( $N_2$ ) environment by using thermogravimetric analyzer (TGA, SQ8-STA8000, Netherlands) and samples were scanned in the range of 50 through 700 °C at a heating rate of 10 °C/min. Proton NMR spectra of LPCL, LPCL-PMPI, LPCL-SDF-1 $\alpha$  and SDF-1 $\alpha$  peptide were collected by using Bruker 400 MHz NMR spectrometer. The LPCL, LPCL-PMPI, and LPCL-SDF-1 $\alpha$  were dissolved in deuterated chloroform ( $CD_3Cl$ ), while SDF-1 $\alpha$  peptide was dissolved in DMSO- $d_6$ .

## 2.3. In vitro cell study

### 2.3.1. Fabrication of electrospun membranes

For *in vitro* assessment of the biocompatibility, two-dimensional microfibrillar membranes were fabricated by electrospinning. Briefly, HPCL was dissolved in a mixture of chloroform/methanol (5:1, v/v) to afford a 15% w/v solution. LPCL-BP, LPCL-SDF-1 $\alpha$  (10 mg/mL of total solution), or LPCL-BP with LPCL-SDF-1 $\alpha$  (10 mg/mL of total solution, 5 mg/mL for each) were mixed along with the HPCL to fabricate HPCL/LPCL-BP, HPCL/LPCL-SDF-1 $\alpha$ , and HPCL/LPCL-BP/LPCL-SDF-1 $\alpha$  membranes. Electrospinning was performed by using the following conditions: (a) voltage, 8 kV, (b) needle-to-collector distance, 10 cm, (c) needle size, 21 G, (d) stainless steel rotating mandrel (diameter = 100 mm), and (e) flow rate, 2 mL/h. The membranes were dried in vacuum for up to 3 days, then cut into circular shape (diameter = 10 mm) and sterilized by ultraviolet (UV) overnight.

### 2.3.2. Cytocompatibility assay

Human umbilical vein endothelial cells (HUVECs) were used to test the bioactivity of microfibrillar membranes. The HUVECs were cultured in an endothelial cell medium (ECM) and harvested at 90% confluency. The membranes were placed into 48-well plates and HUVECs were seeded at a density of  $1 \times 10^4$  cells per well. At day 3 and 5, cell survival was investigated by using live/dead staining assay. Morphological analysis of cell-seeded membranes was carried out by using SEM images

at day 3.

### 2.3.3. Cell proliferation assay

Cell proliferation was evaluated by CCK-8 assay. The membranes were placed into 48-well plates and HUVECs were seeded at a density of  $8 \times 10^3$  cells per well. At day 1, 3, and 5, CCK-8 assay was performed. The optical density (OD) value at 450 nm was measured by the microplate reader (Bio-Rad).

## 2.4. In vivo animal implantation

### 2.4.1. Fabrication of small-diameter vascular grafts

Since vascular grafts should exhibit satisfactory mechanical properties, LPCL was blended along with HPCL by co-electrospinning, the HPCL has been widely exploited for the fabrication of vascular grafts [38,39]. Grafts containing peptides were fabricated by mixing the appropriate proportions of HPCL and LPCL-BP or LPCL-SDF-1 $\alpha$  peptide-polymer conjugates. A total of 4 groups of vascular grafts were fabricated, including (a) HPCL, (b) HPCL + LPCL-BP (HPCL/LPCL-BP), (c) HPCL + LPCL-SDF-1 $\alpha$  (HPCL/LPCL-SDF-1 $\alpha$ ), and (d) HPCL + LPCL-BP + LPCL-SDF-1 $\alpha$  (HPCL/LPCL-BP/LPCL-SDF-1 $\alpha$ ). Briefly, to fabricate HPCL vascular grafts, 2500 mg of HPCL was dissolved in 10 mL of chloroform/methanol (5:1 v/v) to afford 25% (w/v) solution. For HPCL/LPCL-BP or HPCL/LPCL-SDF-1 $\alpha$  vascular grafts, 2375 mg of HPCL and 125 mg of LPCL-BP or LPCL-SDF-1 $\alpha$  peptide-polymer conjugates were dissolved. For HPCL/LPCL-BP/LPCL-SDF-1 $\alpha$  vascular grafts, 2375 mg of HPCL, 62.5 mg of LPCL-BP, and 62.5 mg of LPCL-SDF-1 $\alpha$  peptide-polymer conjugates were dissolved. All groups were spun by using below conditions: (a) voltage, 11 kV, (b) needle-to-collector distance, 12 cm, (c) needle size, 21 G, (d) stainless steel rotating mandrel (diameter, 2.0 mm), and (e) flow rate, 8 mL/h. Vascular grafts (wall thickness, 500  $\mu$ m and diameter, 2.0 mm) were dried in vacuum for up to 3 days, and sterilized by UV before *in vivo* implantation.

### 2.4.2. Characterization of small-diameter vascular grafts

Morphological analysis of grafts was observed by using SEM (Quanta200, Prague, Czech Republic). The average pore size and fiber diameter was measured by using SEM micrographs. At least 5 random fibers or pores per image, 3 images per sample, and 3 samples per group were measured by using NIH Image J software.

Instron Universal Tensile Tester (Instron 5865, MA, USA) was employed to measure the mechanical properties of vascular grafts (length, 3 cm,  $n = 3$ ). The gauge length was set as 10 mm, and samples were subjected to longitudinal extension at a strain rate of 10 mm/min until rupture. The stress - strain curves, maximum stress, and elongation at break were recorded. The elastic modulus was calculated based on the slope of the stress - strain curve in the elastic region [40].

### 2.4.3. Implantation of vascular grafts

Vascular grafts were transplanted into rat abdominal aorta for up to 4 weeks. Sprague-Dawley rats (male, 280–320 g) were obtained from the Laboratory Animal Center of the Academy of Military Medical Sciences (Beijing, China). All animal experiments were approved by the Ethical Committee for the Animal Experiments, Nankai University, Tianjin, China and were followed by the Guide for Care and Use of Laboratory Animals. The implantation procedure was performed as described previously [41]. The rats were randomly divided into 4 groups (HPCL, HPCL/LPCL-BP, HPCL/LPCL-SDF-1 $\alpha$ , HPCL/LPCL-BP/LPCL-SDF-1 $\alpha$ ). Four animals were performed per group. Rats were anesthetized using 1% pentobarbital sodium (10 mg/kg of body weight) by intraperitoneal injection. Before surgery, heparin (100 U/kg) was injected through the tail vein for anticoagulation.

The patency of the implanted vascular grafts was discerned by using Doppler ultrasound (Vevo 2100, Visual Sonics, Toronto, Canada). Vascular grafts with normal blood flow, no occlusion, thrombus or aneurysm were defined as being patent.

## 2.5. Evaluation of the explanted grafts

### 2.5.1. Animal and sample collection

At 4 weeks after the implantation of vascular grafts, animals were sacrificed by an overdose injection of 1% pentobarbital sodium. The explanted grafts were washed with 0.9% NaCl solution and cut into two parts from the middle. One part was embedded in optimal cutting temperature (OCT) for cross-sectioning. The other part was longitudinally cut into three pieces; One piece was embedded in OCT for longitudinal-sectioning, another piece was used for *enface* immunofluorescence staining, and the other piece was prepared for SEM observation.

### 2.5.2. Morphological analysis of explanted grafts

The explanted grafts were fixed by using 2.5% glutaraldehyde overnight and dehydrated by graded ethanol (5 min each). Dried samples were sputter-coated with gold and examined by SEM. Three replicate samples in each group, and nine random fields were photographed for every sample.

### 2.5.3. *Enface* immunofluorescence staining

The samples were washed with PBS and incubated with 5% goat serum for up to 45 min at room temperature (RT). Thereafter, the samples were incubated in CD31 primary antibody (1:100 with PBS) overnight at 4 °C and incubated in the secondary antibody (1:200 with PBS) for 2 h at RT. Finally, samples were mounted with DAPI and observed by Confocal laser scanning microscope (LSM 800, Zeiss, Germany). Nine random fields were captured at anastomotic, quarter, and midportion for each sample. The elongation factor was quantified using CD31 *enface* staining images of the midportion of explants. Briefly, the length of CD31<sup>+</sup> cells was divided by their width for elongation factor [6]. The higher the factor is, the mature the ECs is.

### 2.5.4. Histological staining

The samples for cross-sectioning or longitudinal-sectioning were cut into 6 μm thick slides at −20 °C. The histological staining (H&E, Safranin O, Masson's Trichrome, and VVG) were performed by following the introduction manual step. Bright field microscope (Leica DM3000, Germany) was used for imaging of the slides after staining.

### 2.5.5. Immunofluorescence staining

Prior to the immunofluorescence staining, the slides were fixed in cold acetone for 10 min and washed with PBS. For cell surface antigen staining, the sections were incubated with 5% goat serum for 45 min at RT to block non-specific protein adsorption. For intracellular antigen staining, the permeation of cell membrane was carried out by using 0.1% Triton-PBS before blocking by the serum. Sections were incubated in primary antibodies overnight at 4 °C, followed by incubation in secondary antibodies for 2 h at RT. Sections incubated only with the PBS were used as negative controls. Finally, the sections were mounted with DAPI and observed by upright fluorescence microscope (Axio Imager Z1, Zeiss, Germany). The VPCs were stained by using anti-Sca-1 antibody (1:100), and the numbers of Sca-1<sup>+</sup> cells infiltrated into the graft wall were quantified by using the high-magnification field of graft wall (200 × ). The staining for ECs and neo-vessels was performed by using anti-CD31 (1:100) antibody. The endothelium coverage rate was calculated by the length of the EC layer to the total graft length in the longitudinal-section. The numbers of neo-vessels were measured by using the high-magnification field of graft wall (200 × ). The SMCs were stained by using anti-α-SMA (1:100) and anti-MYH11 (1:100) primary antibodies. The average thickness was calculated as the area of the positive cells divided by the length of the SMC layer in the luminal area. For inflammatory cell recruitment, sections were incubated with anti-CD68 (1:100), anti-iNOS (1:100), and anti-CD206 (1:100) primary antibodies to identify total macrophages, M1 (pro-inflammatory) and M2 (anti-inflammatory) macrophages, respectively. The numbers of cells

were measured by using the high-magnification field of graft wall (400 × ).

## 2.6. Statistical analysis

At least three samples were performed for the quantitative analysis. Data were expressed as mean ± SEM and analyzed by GraphPad Prism 7 Software. Comparisons between multiple groups were performed by using one-way analysis of variance (ANOVA) followed by Tukey's multiple comparisons test. The  $p < 0.05$  was considered statistically significant.

## 3. Results

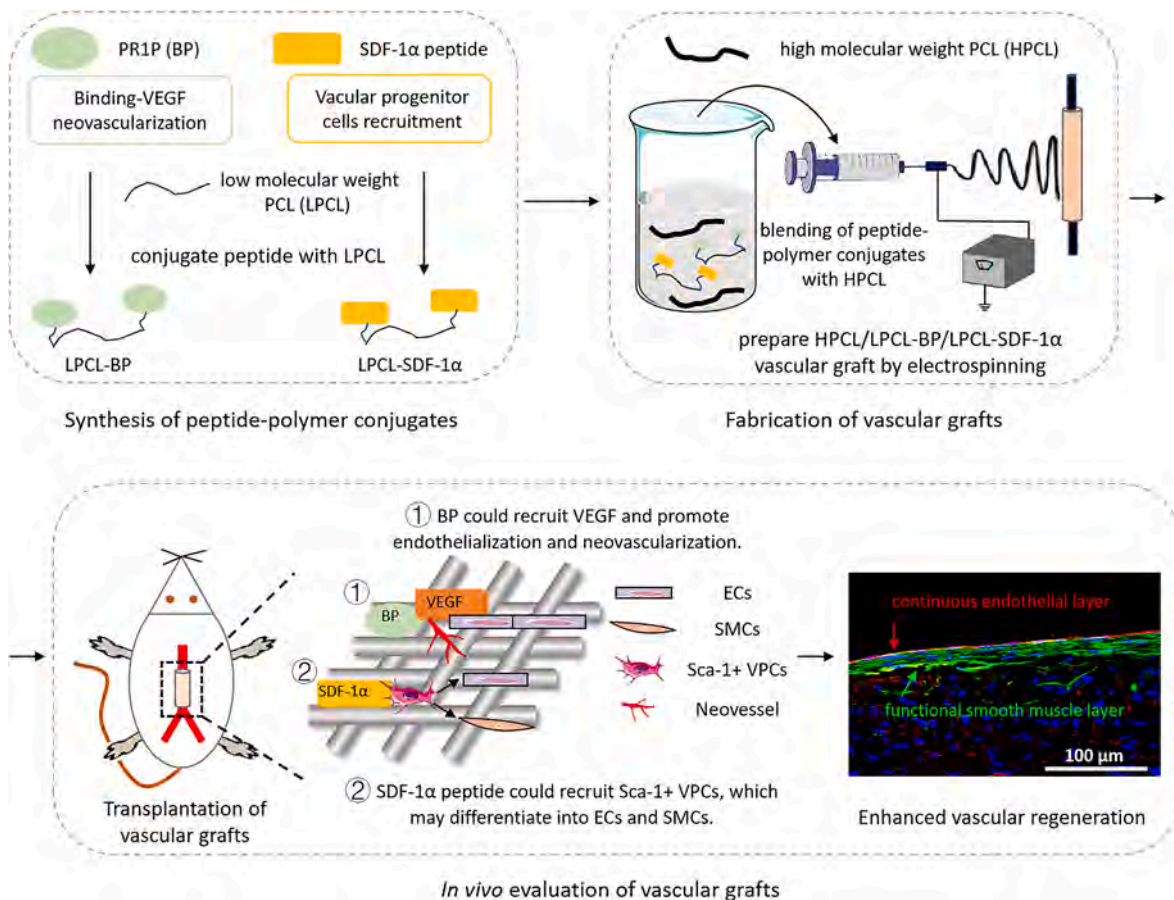
LPCL was modified with SDF-1α peptide and BP to simultaneously recruit endogenous stem/progenitor cells as well as VEGF *in situ*. The bioactive peptide-polymer conjugates were next blended along with the HPCL to afford electrospun membranes for *in vitro* studies and small-diameter vascular grafts for *in vivo* implantation. Vascular grafts were implanted into rat abdominal aorta for up to 4 weeks and were examined for endogenous cell infiltration, endothelialization, and vascular remodeling (Scheme 1).

### 3.1. Structural analysis

Fig. 1a showed the schematic illustration of the conjugation of peptides with LPCL polymers. FTIR spectra were recorded to discern the difference between the LPCL and LPCL-BP or LPCL-SDF-1α (Fig. 1b). LPCL spectra exhibited peaks at 2940 cm<sup>-1</sup>, 2840 cm<sup>-1</sup>, 1718 cm<sup>-1</sup>, 1294 cm<sup>-1</sup>, and 1242 cm<sup>-1</sup>, which were ascribed to the asymmetric CH<sub>2</sub> stretching, symmetric CH<sub>2</sub> stretching, carbonyl stretching, and C–O stretching [19]. While both LPCL-BP and LPCL-SDF-1α displayed these peaks, they showed additional bands in the range of 3729–3024 cm<sup>-1</sup>, 1658 cm<sup>-1</sup>, and 1506 cm<sup>-1</sup>. These additional peaks are ascribed to the N–H stretching as well as amide I and amide II bands due to the incorporation of peptides. The XPS was further performed to assess the modification of LPCL with peptides. The XPS pattern of LPCL revealed typical peaks corresponding to the O1s and C1s in the range of 536–530 and 290–282 eV, respectively. The LPCL-BP and LPCL-SDF-1α exhibited the above mentioned peaks and in addition displayed a peak at 400 eV, which is ascribed to the N1s (Fig. 1c) [42]. These results indicate successful grafting of peptides with the LPCL.

The synthesis steps were further monitored by collecting the proton NMR spectra. The <sup>1</sup>H NMR spectrum of LPCL is shown in Fig. S1a. Proton assignments of PMPI and LPCL-PMPI were based on published spectra for PMPI and LPCL [37]. The NMR spectra of LPCL-PMPI showed the successful conjugation of LPCL to PMPI to afford LPCL-maleimide, which exhibited chemical shifts between 6.5 and 8 ppm (Fig. S1b). The chemical shifts confirming the successful synthesis of LPCL-maleimide included 7.6 ppm (4H orthogonal to maleimide, 2), 7.3 ppm (4H, aromatic H orthogonal to maleimide, 2'), and 6.9 ppm (4H, maleimide vinyl, 1). The NMR spectrum of LPCL-SDF-1α was further ascertained (Fig. S1c). In addition to the characteristic peaks of the LPCL, the additional peaks attributable to SDF-1α peptide were found in the spectrum of the LPCL-SDF-1α. Moreover, the disappearance of the maleimide peak at 6.9 ppm indicated a successful reaction between the maleimide on the LPCL-PMPI and the thiol on the peptide. The <sup>1</sup>H NMR spectrum of SDF-1α peptide is shown in Fig. S1d.

To gain a further insight into the effect of the modification of LPCL with peptides, TGA was performed. The obtained results revealed that the peptides' tethering lowered the thermal stability of pristine LPCL (Fig. 1d). This reduction in the thermal stability can be ascribed to the fact that the peptides can degrade at lower temperature than that of the pristine LPCL. Shin et al. also observed similar TGA trends in arginine-glycine-aspartic acid (RGD)-conjugated PLGA scaffolds [43]. Briefly, LPCL exhibited 5, 10, 20, 30, 40, and 50% mass loss at 276, 298, 327,



**Scheme 1.** Schematic illustration of the synthesis of peptide-polymer conjugates, fabrication of vascular grafts, and *in vivo* evaluation of vascular grafts.

358, 392, and 406 °C. LPCL-BP displayed 5, 10, 20, 30, 40, and 50% mass loss at 280, 312, 330, 339, 351, and 364 °C. On the other hand, LPCL-SDF-1 $\alpha$  exhibited 5, 10, 20, 30, 40, and 50% mass loss at 275, 296, 316, 324, 332, and 339 °C.

### 3.2. Cytocompatibility of scaffolds

We ascertained the cytocompatibility of membranes by live/dead cell assay and cell proliferation assay *in vitro*. HUVECs were seeded on electrospun HPCL, HPCL/LPCL-BP, HPCL/LPCL-SDF-1 $\alpha$ , and HPCL/LPCL-BP/LPCL-SDF-1 $\alpha$  membranes for up to day 5. As can be seen from Fig. 2, cells grew nicely on all membranes. The cell number further rose at day 5, especially on HPCL/LPCL-SDF-1 $\alpha$ , and HPCL/LPCL-BP/LPCL-SDF-1 $\alpha$  membranes (Fig. 2a). Similarly, cell proliferation was significantly higher in the HPCL/LPCL-SDF-1 $\alpha$  and HPCL/LPCL-BP/LPCL-SDF-1 $\alpha$  groups as compared to that of HPCL and HPCL/LPCL-BP groups at 3 and 5 days (Fig. 2b). SEM images further revealed that cell spreading on HPCL/LPCL-BP, HPCL/LPCL-SDF-1 $\alpha$  and HPCL/LPCL-BP/LPCL-SDF-1 $\alpha$  membranes was superior to that on the HPCL membranes (Fig. 2c).

### 3.3. Morphological analysis and mechanical properties of vascular grafts

Having ascertained the cytocompatibility of membranes *in vitro*, we fabricated electrospun small-diameter vascular grafts by mixing bioactivated LPCL-BP, LPCL-SDF-1 $\alpha$ , or both LPCL-BP and LPCL-SDF-1 $\alpha$  along with HPCL (Scheme 1). As can be observed from the gross morphology, the tubular-shaped small-diameter vascular grafts were successfully prepared by electrospinning (Fig. 3a). The grafts exhibited microfibers, the average fiber diameter was  $5.64 \pm 0.44 \mu\text{m}$ ,  $6.26 \pm 0.54 \mu\text{m}$ ,  $6.24 \pm 0.44 \mu\text{m}$ , and  $6.47 \pm 0.37 \mu\text{m}$  in HPCL, HPCL/LPCL-BP, HPCL/LPCL-SDF-1 $\alpha$ , and HPCL/LPCL-BP/LPCL-SDF-1 $\alpha$  groups,

respectively. Similarly, the pore size was found to be  $34.51 \pm 4.51 \mu\text{m}$ ,  $40.41 \pm 4.48 \mu\text{m}$ ,  $41.60 \pm 5.13 \mu\text{m}$ , and  $41.86 \pm 4.35 \mu\text{m}$  for HPCL, HPCL/LPCL-BP, HPCL/LPCL-SDF-1 $\alpha$ , and HPCL/LPCL-BP/LPCL-SDF-1 $\alpha$  groups, respectively (Fig. 3b). The bioactive HPCL grafts showed slightly higher fiber diameter and pore size than that of the pure HPCL grafts, as peptide-polymer exhibit low molecular weight, their incorporation into HPCL may lower the viscosity and surface charge density of the solution, which can also influence the fiber morphology [44]. SEM images of the graft wall further revealed porous morphology of grafts both at the cross-section (designated as 1) and inner surface (designated as 2) (Fig. 3c). Water contact angle (WCA) measurement also revealed an insignificant difference in four groups, which displayed almost similar WCA, thereby indicating that the blending of HPCL with peptide-LPCL conjugates did not influence hydrophilicity/hydrophobicity of vascular grafts (Fig. S2). The tensile properties of vascular grafts were further examined. While all of the grafts exhibited typical stress-strain curves (Fig. 3d), they did not significantly differ in terms of the tensile properties, including Young's modulus, max stress and elongation at break (Fig. 3e-g).

### 3.4. Implantation of vascular grafts

We next transplanted vascular grafts into rat abdominal aorta for 4 weeks (Fig. 4a). A total of 4 grafts were implanted for each group. Upon implantation, vascular grafts did not reveal any blood leakage and allowed the smooth flow of the blood. Fig. 4b showed the photographs of vascular grafts just after implantation and 4 weeks after implantation. Doppler ultrasound was next leveraged to discern the patency of implanted vascular grafts, the blood flow can be detected at the anastomosis sites as well as the other portions of the grafts, which are indicative of the good patency of grafts. A representative image of

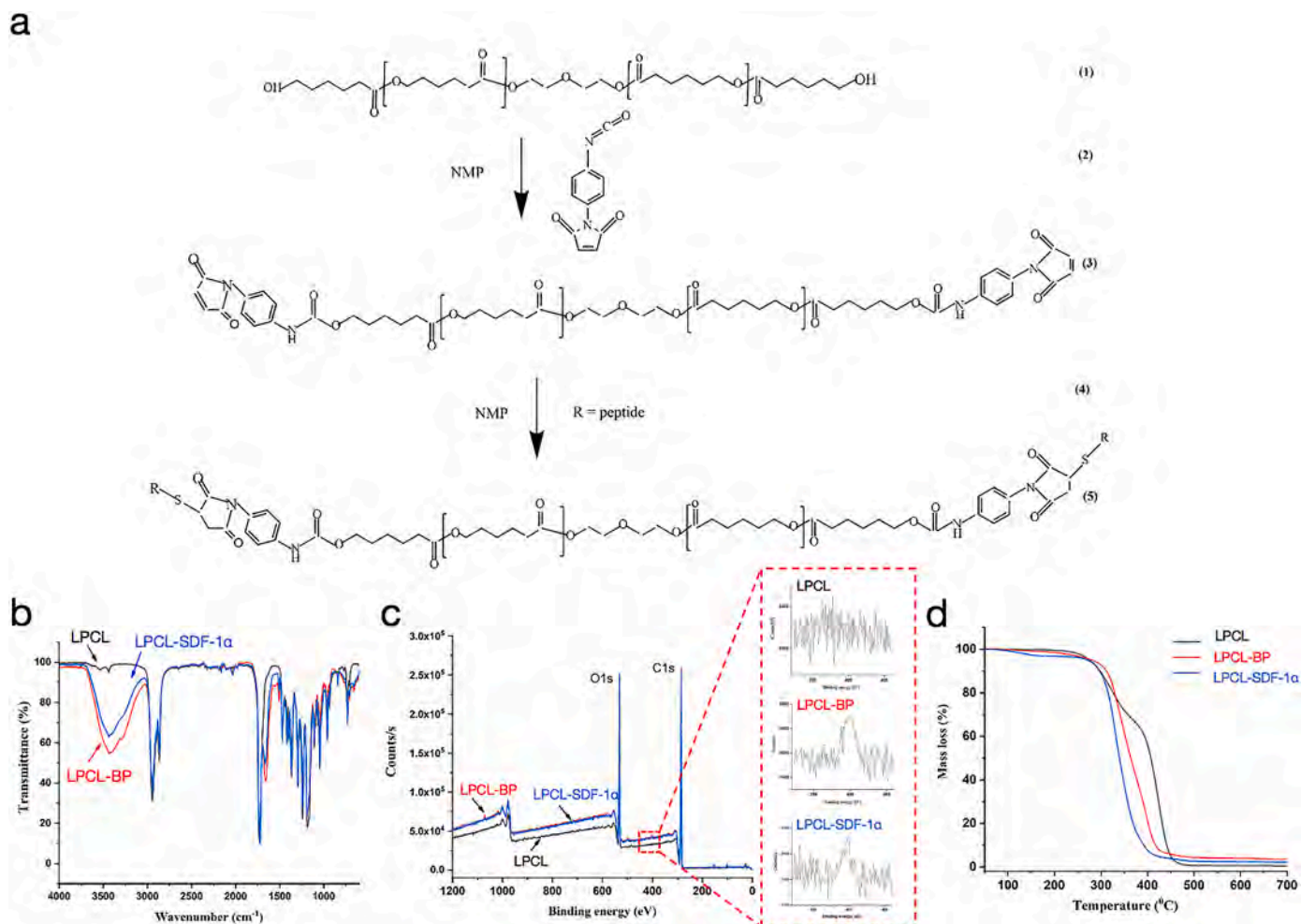


**Fig. 1.** Preparation and characterization of peptide-polymer conjugates. (a) Schematic illustration of the synthesis routes of LPCL-BP and LPCL-SDF-1 $\alpha$ . (b) FT-IR spectra of LPCL, LPCL-BP, and LPCL-SDF-1 $\alpha$ . Peptide modified polymers showed distinctive peaks in the range of 3000–3500 cm<sup>-1</sup>, indicative of the N–H and O–H bonds. Peptides sequence for BP and SDF-1 $\alpha$  is CGDRVQRQTTTVVA and CGSKPVVLSYR, respectively. (c) XPS spectra of LPCL, LPCL-BP and LPCL-SDF-1 $\alpha$ . Peptide modified polymers showed distinctive N peaks at 400 eV, indicative of the conjugation of peptides. (d) Thermogravimetric analysis of LPCL, LPCL-BP, and LPCL-SDF-1 $\alpha$ . Peptide modified polymers exhibited lower thermal stability than that of the pristine LPCL polymers.

HPCL/LPCL-BP/LPCL-SDF-1 $\alpha$  grafts was shown in Fig. 4c, which revealed unperturbed blood flow by the red colour. The 3 out of a total 4 grafts remained patent in HPCL, HPCL/LPCL-BP, and HPCL/LPCL-SDF-1 $\alpha$  groups (patency rate, 75%). On the other hand, all grafts were found to be patent in the HPCL/LPCL-BP/LPCL-SDF-1 $\alpha$  group (Fig. 4d). Stereoscopic pictures revealed the implanted vascular grafts maintained their structural stability without an obvious collapse or an aneurysm (Fig. 4e). HPCL/LPCL-BP, HPCL/LPCL-SDF-1 $\alpha$ , and HPCL/LPCL-BP/LPCL-SDF-1 $\alpha$  grafts exhibited neat lumen surface without the accumulation of a thrombotic species. The explants were decellularized using collagenase I and evaluated by SEM for fibers morphology. Four groups of vascular grafts did not significantly differ in term of degradation after 4 weeks of implantation (Fig. S3). While HPCL exhibits degradation period for up to 1–2 years [45], the LPCL-BP or LPCL-SDF-1 $\alpha$  were used only in small amount, which did not induce a noticeable degradation *in vivo*.

### 3.5. Cell infiltration

The explanted grafts were next subjected to histological and immunofluorescence staining to gain a further insight into cellular infiltration and vascular remodeling (Fig. 5). The H&E staining revealed significant infiltration of host cells, and the formation of neo-tissues on the luminal side in the HPCL/LPCL-BP, HPCL/LPCL-SDF-1 $\alpha$ , and HPCL/LPCL-BP/

LPCL-SDF-1 $\alpha$  grafts as compared to that of the HPCL grafts (Fig. 5a). The luminal diameter was similar in all groups (Fig. 5b). The excellent regeneration of neo-tissues in the graft wall and luminal side of bio-activated HPCL grafts is ascribed to the incorporated peptides, which may encourage the mobilization and recruitment of host cells as well as the formation of neo-vessels. We performed DAPI staining to quantify the numbers of infiltrated cells for up to a distance of 0 through 200  $\mu$ m from the luminal side of the grafts (Fig. 5c). As can be seen from Fig. 5d, HPCL/LPCL-BP and HPCL/LPCL-BP/LPCL-SDF-1 $\alpha$  grafts displayed significantly higher numbers of cells than that of the HPCL grafts, the infiltrated cells in HPCL/LPCL-BP also significantly higher than that in HPCL/LPCL-SDF-1 $\alpha$  grafts. Since SDF-1 $\alpha$  can mobilize VPCs, which can participate in tissue regeneration, we further performed staining for Sca-1 antibody (Fig. 5e). The quantitative analysis revealed significantly higher numbers of Sca-1<sup>+</sup> VPCs in HPCL/LPCL-SDF-1 $\alpha$  and HPCL/LPCL-BP/LPCL-SDF-1 $\alpha$  grafts as compared to that of the HPCL and HPCL/LPCL-BP grafts (Fig. 5f). To further illustrate if these Sca-1<sup>+</sup> VPCs can differentiate into ECs and SMCs, we carried out co-staining for Sca-1/CD31 and Sca-1/ $\alpha$ -SMA antibodies for all of the grafts (Fig. 5g and h). The co-immunofluorescence staining revealed the infiltration of Sca-1<sup>+</sup>/CD31<sup>+</sup> cells as well as Sca-1<sup>+</sup>/ $\alpha$ -SMA<sup>+</sup> cells, which may have implications for endogenous VPCs mediated rapid endothelialization and vascular remodeling of cell-free vascular grafts.

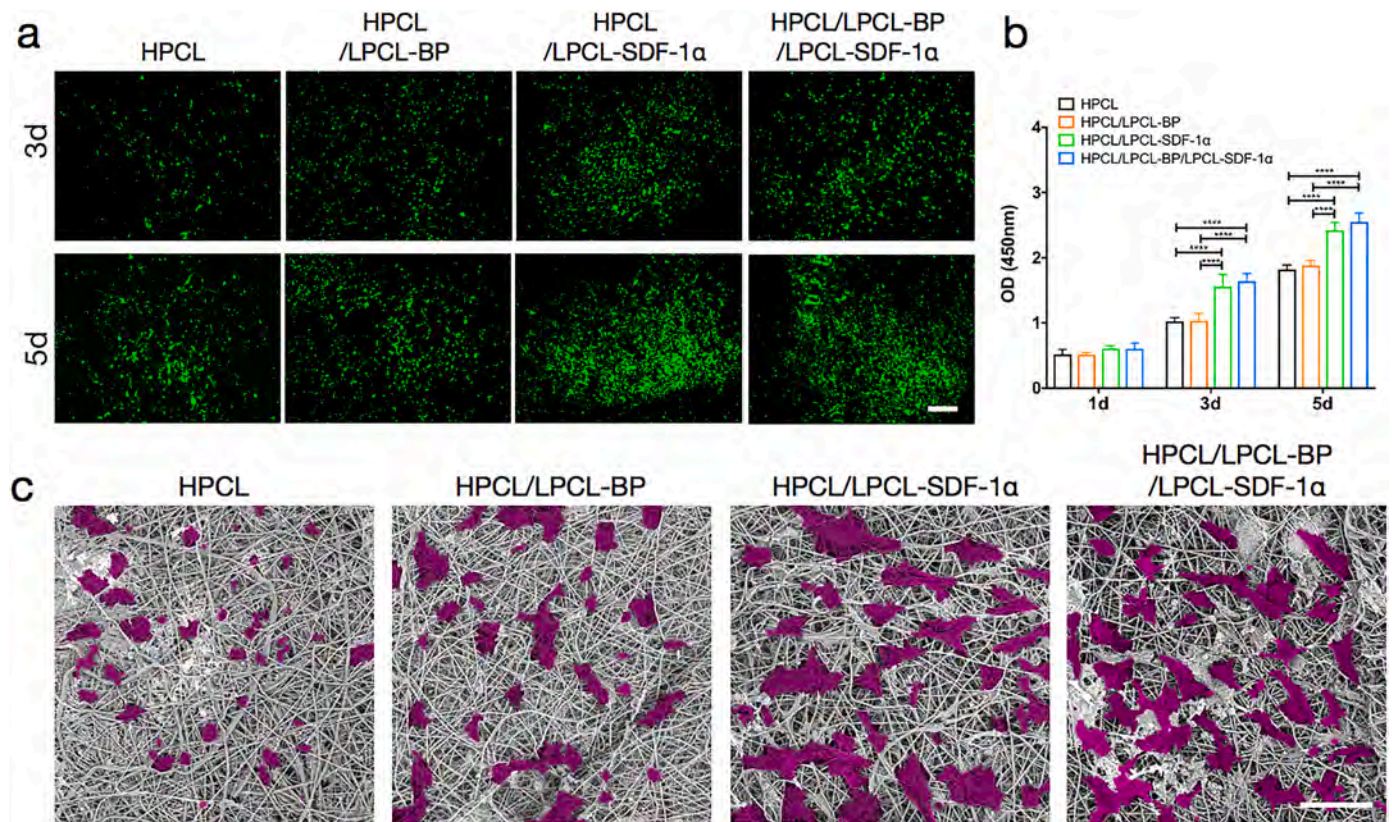


**Fig. 2.** Cell viability on HPCL, HPCL/LPCL-BP, HPCL/LPCL-SDF-1 $\alpha$  and HPCL/LPCL-BP/LPCL-SDF-1 $\alpha$  membranes. HUVECs were seeded onto membranes and cultured for 1, 3, and 5 days. (a) A live/dead assay was performed at days 3 and 5. Scale bar, 500  $\mu$ m. (b) Cell proliferation on scaffolds was determined by the CCK8 assay at day 1, 3, and 5. (c) Morphological analysis of HUVECs cultured membranes at day 3 by SEM images. Scale bar, 80  $\mu$ m. The SDF-1 $\alpha$  and dual-peptide tethered membranes exhibited significantly higher cell viability as compared to HPCL and HPCL/LPCL-BP membranes. \* $P < 0.05$ .

### 3.6. Rapid endothelialization of vascular grafts

Since endothelium plays a pivotal role both for the short-term and long-term patency of vascular grafts, we analyzed the endothelialization of vascular grafts, especially investigated four different areas, including anastomotic, quarter portion, mid portion and graft wall, as shown in Fig. 6a. SEM images for the luminal side of the HPCL/LPCL-BP, HPCL/LPCL-SDF-1 $\alpha$ , and HPCL/LPCL-BP/LPCL-SDF-1 $\alpha$  grafts showed the nice regeneration of ECs, which displayed cobblestone-like morphology and were elongated in the direction of the blood flow (Fig. 6b). However, the images of the HPCL hardly showed ECs at the mid portion, the morphology of microfibers can be observed at the luminal side of HPCL grafts (Fig. 6b). Intriguingly, *enface* immunofluorescence staining of vascular grafts showed ECs in the HPCL/LPCL-SDF-1 $\alpha$ , and HPCL/LPCL-BP/LPCL-SDF-1 $\alpha$  grafts were elongated (Fig. 6c). Immunofluorescence staining of longitudinal section by CD31 antibody also showed the nice regeneration of ECs and the formation of neo-vessels at the anastomotic as well as quarter portion and mid portion of grafts in peptides modified groups (Fig. 6d). The HPCL/LPCL-BP, HPCL/LPCL-SDF-1 $\alpha$ , and HPCL/LPCL-BP/LPCL-SDF-1 $\alpha$  grafts exhibited significantly higher endothelium coverage than that of the HPCL grafts. The latter displayed endothelium coverage for up to 50% (Fig. 6e). Meanwhile, in HPCL/LPCL-SDF-1 $\alpha$  and HPCL/LPCL-BP/LPCL-SDF-1 $\alpha$  group, the elongation factor for ECs at midportion of grafts was significantly higher than that of the HPCL/LPCL-BP grafts, while the ECs was undetected at mid portion in the HPCL grafts (Fig. 6f). The HPCL/LPCL-BP and HPCL/LPCL-BP/LPCL-SDF-1 $\alpha$  grafts exhibited higher numbers of neo-vessels in graft wall as compared to that of the HPCL grafts (Fig. 6g). Taken together, the bioactive grafts not only displayed greater endothelium coverage but also exhibited more numbers of neo-vessels in the grafts wall and

elongated ECs in the mid portion of the grafts. These data reveal that the bioactivated HPCL can successfully promote endothelialization of the grafts.

### 3.7. Regeneration of smooth muscle layer

In addition to the rapid endothelialization, SMCs regeneration plays a crucial role for vascular remodeling. The explants were stained with SMCs markers, including  $\alpha$ -SMA and MYH11 to gain an insight into SMCs regeneration and vascular remodeling as well as determine the synthetic and contractile phenotypes of SMCs, respectively [46]. Fig. 7a showed the  $\alpha$ -SMA staining of vascular grafts, which not only showed the regeneration of SMCs on the luminal side but also within the graft wall. HPCL/LPCL-SDF-1 $\alpha$  and HPCL/LPCL-BP/LPCL-SDF-1 $\alpha$  groups displayed nice regeneration of  $\alpha$ -SMA positive cells in the luminal and abluminal sides of the explanted grafts. The quantitative analysis further indicated significantly higher thickness of  $\alpha$ -SMA positive neo-tissues in the HPCL/LPCL-BP/LPCL-SDF-1 $\alpha$  grafts than that of the HPCL grafts (Fig. 7b). Meanwhile, explants showed significant regeneration of MYH11<sup>+</sup> SMCs in HPCL/LPCL-SDF-1 $\alpha$  and HPCL/LPCL-BP/LPCL-SDF-1 $\alpha$  grafts as compared to that of the HPCL grafts (Fig. 7c and d). More importantly, double-immunofluorescence staining by using CD31/ $\alpha$ -SMA revealed the regeneration of well-organized CD31<sup>+</sup> ECs and  $\alpha$ -SMA<sup>+</sup> SMCs in the HPCL/LPCL-BP/LPCL-SDF-1 $\alpha$  grafts (Fig. S4). To gain a further insight into the regeneration of ECM components, explanted grafts were stained with Masson's trichrome, VVG, and Safranin O for collagen, elastin, and glycosaminoglycans (GAGs) regeneration, respectively. Native aorta sections were also stained for comparison. As can be observed from Fig. 7e-g, native aorta displayed oriented collagen and elastin fibrils as well as GAGs in the tunica media.

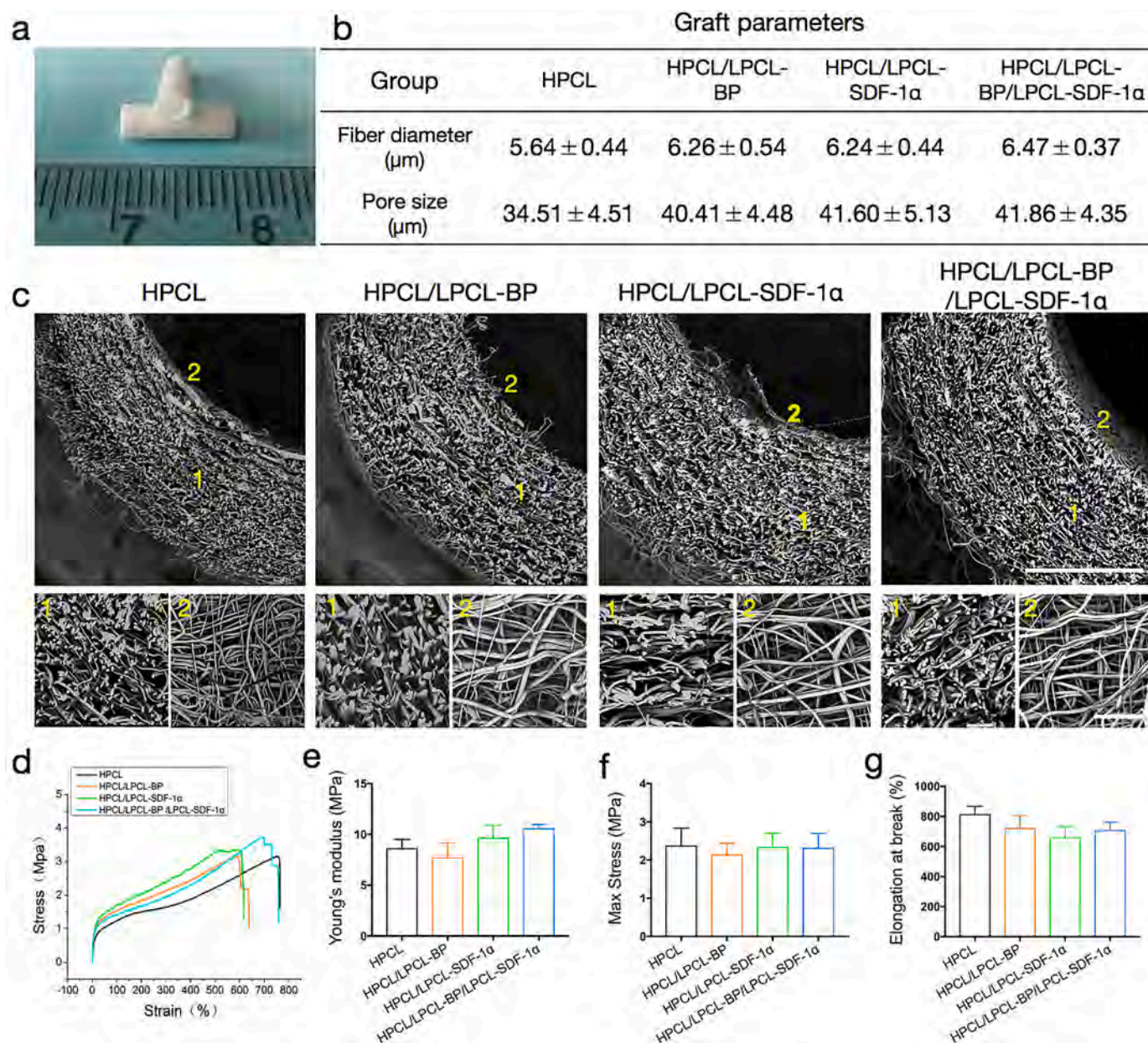


**Fig. 3.** Fabrication and characterization of HPCL, HPCL/LPCL-BP, HPCL/LPCL-SDF-1 $\alpha$  and HPCL/LPCL-BP/LPCL-SDF-1 $\alpha$  vascular grafts. (a) Images show the tubular vascular grafts (2.0 mm in inner diameter, 500  $\mu\text{m}$  in thickness, and 1.0 cm in length). (b) The graft parameters are summarized. (c) Representative SEM images of vascular grafts (upper panel). Lower panel were magnified images of cross-section and inner surface of vascular grafts as indicated by 1 and 2 in the upper panel. Scale bars, 500  $\mu\text{m}$  or 100  $\mu\text{m}$  (magnified images). (d) Representative stress-strain curves of vascular grafts. Mechanical characterization ( $n = 3$ ) of various grafts in longitudinal direction for Young's modulus (e), maximum stress (f) and elongation at break (g).

On the other hand, while the HPCL grafts lacked the deposition of ECM components, grafts containing peptides displayed substantial regeneration of ECM components. Especially, the HPCL/LPCL-BP/LPCL-SDF-1 $\alpha$  grafts revealed nice regeneration of collagen as well as elastin and GAGs in a fashion similar to the native arteries.

### 3.8. Inflammatory response

Since upon *in vivo* implantation, vascular grafts are accumulated by the different types of inflammatory cell types, which further influence vascular remodeling. In this study, vascular grafts were stained with different markers for the inflammatory cell types, such as CD68, iNOS, and CD206 for total, M1, and M2 macrophages, respectively (Fig. 8). Four types of grafts did not significantly differ in terms of the numbers of CD68<sup>+</sup> macrophages (Fig. 8a and d). The HPCL/LPCL-BP and HPCL/

LPCL-SDF-1 $\alpha$  grafts exhibited significantly more numbers of iNOS<sup>+</sup> macrophages than that of HPCL grafts (Fig. 8b and e). On the other hand, HPCL/LPCL-BP/LPCL-SDF-1 $\alpha$  grafts exhibited significantly higher numbers of CD206<sup>+</sup> macrophages than that of the HPCL and HPCL/LPCL-BP grafts. Meanwhile, the number of CD206<sup>+</sup> macrophages in HPCL/LPCL-SDF-1 $\alpha$  was also higher than that of HPCL grafts (Fig. 8c and f). Quantitative analysis of the CD206<sup>+</sup>/iNOS<sup>+</sup> cells showed higher ratio of M2/M1 in HPCL/LPCL-BP/LPCL-SDF-1 $\alpha$  grafts than that of the HPCL/LPCL-BP grafts, thereby indicating that the macrophages were polarized from pro-inflammatory to anti-inflammatory phenotypes (Fig. 8g). Dual peptides-loaded grafts exhibited rapid endothelialization and vascular remodeling, which may presumably be attributed to the more number of CD206<sup>+</sup> (M2) macrophages and a higher ratio of M2/M1.

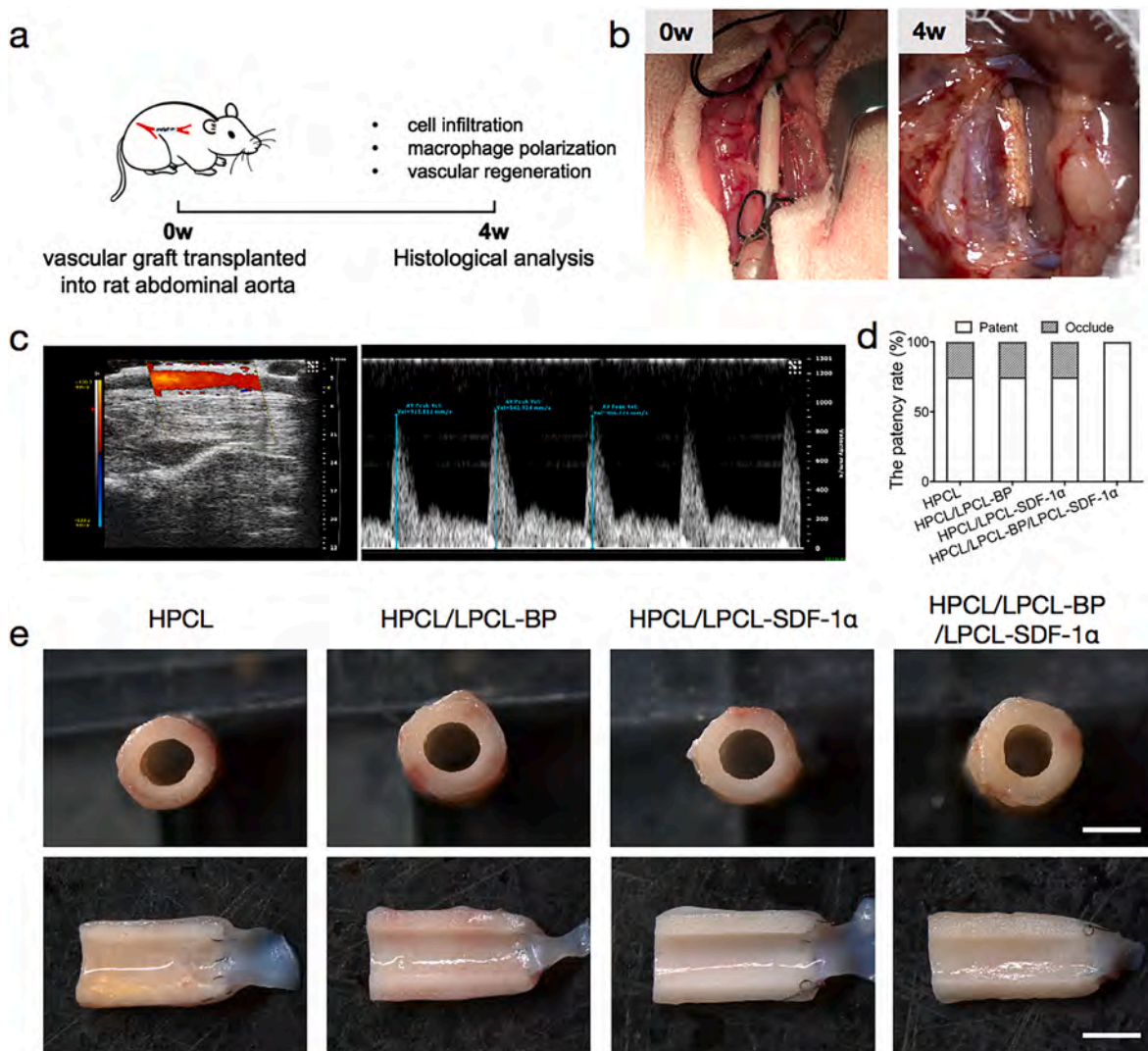


**Fig. 4.** Characterization and *in vivo* performance of vascular grafts utilizing rat abdominal aorta replacement model. (a) Schematic illustration of the *in vivo* evaluation conducted in SD rats. (b) Images of vascular grafts implanted into rat abdominal aorta (left) and integrated with host artery after 4 weeks (right). (c) Representative Doppler ultrasound image of the implanted HPCL/LPCL-BP/LPCL-SDF-1 $\alpha$  vascular graft. (d) Determination of the patency rate of the implanted vascular grafts after 4 weeks,  $n = 4$  animals per group. (e) Representative stereoscopic images of cross section (upper panel) or longitudinal section (lower panel) of vascular grafts at 4 weeks post implantation. Scale bars, 2 mm.

#### 4. Discussion

Autografts are widely accepted for vascular grafting. However, their limited availability hampers their utilization. Alternatively, synthetic vascular grafts fabricated by using different natural and synthetic polymers have been widely investigated. Amongst, synthetic biodegradable polymers, such as PCL, has been widely used in bio-related applications [38]. Nonetheless, the bioinertness of PCL may hamper its applicability for tissue repair, thereby necessitating its bioactivation by using different types of biological cues, including ECM proteins, cytokines, and chemokines [47–49]. Of particular interest are chemokines, such as SDF-1 $\alpha$ , which has been shown to recruit endogenous stem/progenitor cells [32]. Recruited endogenous stem/progenitor cells may differentiate into particular lineages to drive *in situ* tissue repair [30]. Besides, SDF-1 $\alpha$  has been shown to promote endothelialization and vascular remodeling by recruiting EPCs and SMPCs. Despite these obvious advantages, SDF-1 $\alpha$  exhibits short half-life *in vitro* and *in vivo*, which can be easily degraded by Dipeptidyl Peptidase-4 (DPP-4) and MMPs [31]. Besides, being a large molecular weight protein, SDF-1 $\alpha$  is difficult to be synthesized or incorporated into biomaterials. On the

other SDF-1 $\alpha$  analogues, which can replicate the biological features of the full-length protein, have been engineered and incorporated into biomaterials to drive *in situ* tissue repair [31]. Nonetheless, the fast release of these SDF-1 $\alpha$  analogues may obscure their potential therapeutic benefits [33]. Moreover, SDF-1 $\alpha$ -recruited cells may not be easily differentiated into targeted cell types. The VEGF gradients at the injury may not only help promote endothelialization on the luminal side as well as neovascularization in the graft wall but may also help regulate endogenously recruited cells and promote vascular remodeling [20]. However, the bolus delivery of SDF-1 $\alpha$  and VEGF may be insufficient to realize these effects. To circumvent these shortcomings, BP was shown to recruit VEGF *in situ* and promote neovascularization for ligament regeneration [24]. We conjugated BP and SDF-1 $\alpha$  peptide with the LPCL to induce stem cell mobilization and promote neovascularization and endothelialization. The combined effect of BP and SDF-1 $\alpha$  peptides may help promote *in situ* tissue repair and vascular remodeling in electrospun vascular grafts. We leveraged a facile bioconjugation approach by first activating the hydroxyl groups of the LPCL and thereafter conjugating cysteine-tagged peptides with these activated groups. This approach is simple and straightforward, which can be further leveraged to

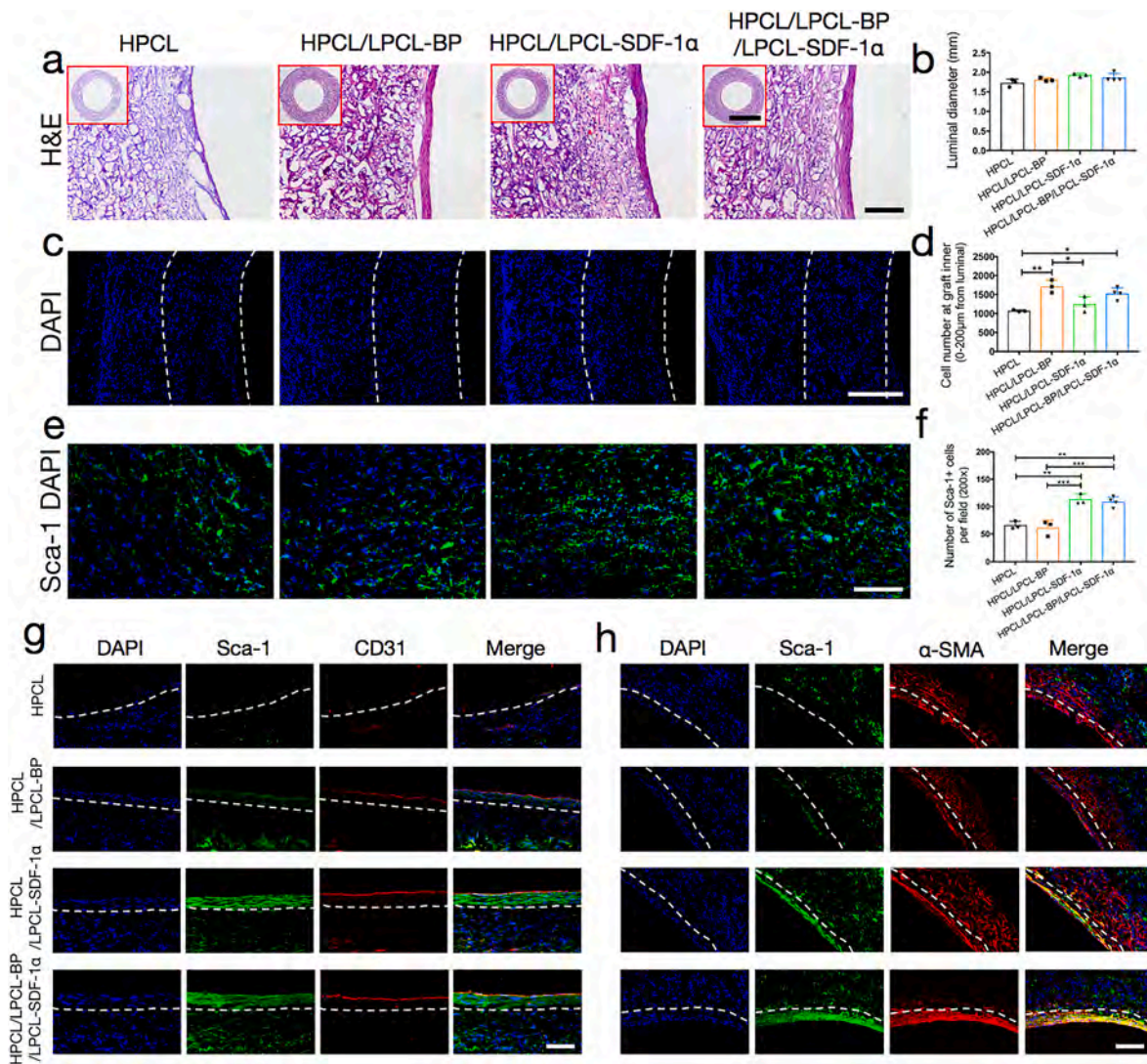


**Fig. 5.** Peptides modification increases the infiltration of VPCs and contributes to endothelialization and smooth muscle regeneration. (a) Representative images of H&E staining on cross-section of vascular grafts. Scale bars, 2 mm or 100  $\mu$ m (magnified images). (b) The luminal diameter of explanted grafts was calculated based on the cross-sections with H&E staining. (c) Immunofluorescence images of DAPI staining (white dashed lines indicate the areas at 0–200  $\mu$ m depths from the graft lumen). Scale bars, 200  $\mu$ m. (d) The cell infiltrated into graft inner wall (0–200  $\mu$ m) were calculated. (e) The distribution of Sca-1<sup>+</sup> VPCs in the vascular graft wall was shown by immunofluorescence staining with Sca-1 antibody. Scale bars, 100  $\mu$ m. (f) The number of Sca-1<sup>+</sup> VPCs within the vascular graft wall was calculated based on Sca-1 immunofluorescence staining (200  $\times$  magnification). (g–h) Co-immunofluorescence staining of Sca-1 (green) and CD31 (red) or  $\alpha$ -SMA (red) on sections of vascular grafts (white dashed lines indicate the luminal region). Scale bars, 100  $\mu$ m \* $P$  < 0.05, \*\* $P$  < 0.01, \*\*\* $P$  < 0.001. (For interpretation of the references to colour in this figure legend, the reader is referred to the Web version of this article.)

incorporate other types of peptides with the polymers to improve their applicability.

Since implantable grafts should enable a supportive environment for cellular growth and neo-tissue formation, the compatibility determination is pivotal. Cytocompatibility evaluation by using cell proliferation and live/dead assay revealed cellular growth on membranes over 5 days *in vitro*. Especially, cells seeded on HPCL/LPCL-SDF-1 $\alpha$  and HPCL/LPCL-BP/LPCL-SDF-1 $\alpha$  membranes grew well at all time points than that of the HPCL and HPCL/LPCL-BP grafts, which may also have implications for the *in vivo* biocompatibility (Fig. 2).

So far, different types of grafts have been fabricated by using a myriad of techniques, such as electrospinning, salt-leaching, and 3D printing [50–53]. Micro/nanofabrication techniques, including electrospinning afford the fabrication of ECM-like scaffolds [54]; the microstructure and morphology of vascular grafts can be further tailored by varying electrospinning parameters. Previously, we have leveraged electrospinning to fabricate microfibrillar vascular grafts, displaying

large pore size. As compared to vascular grafts consisting of thin fibers and small pore size, the grafts composed of thick fibers and large pore size exhibited extensive cellular infiltration as well as induced macrophages modulation toward anti-inflammatory (M2) phenotypes [38,45]. In this study, we fabricated microfibrillar vascular grafts exhibiting a porous morphology (Fig. 3c), thereby replicating the structure of previous PCL-based grafts. Notably, such a porous structure may allow for the infiltration of cells from the luminal as well as abluminal sides. Vascular grafts were next implanted into rat abdominal aorta and evaluated for up to 4 weeks. Since thrombotic complications as well as short-term and long-term stenosis restrict the performance of vascular grafts, the evaluation of thrombi formation and smooth flow of the blood is of considerable significance. Vascular grafts were found to be well-integrated with the host tissues and remain patent and free of thrombotic deposition as revealed by the Doppler ultrasound and stereomicroscope (Fig. 4c, e). The HPCL grafts are composed of thick fibers and large pores, which have already been shown to exhibit good

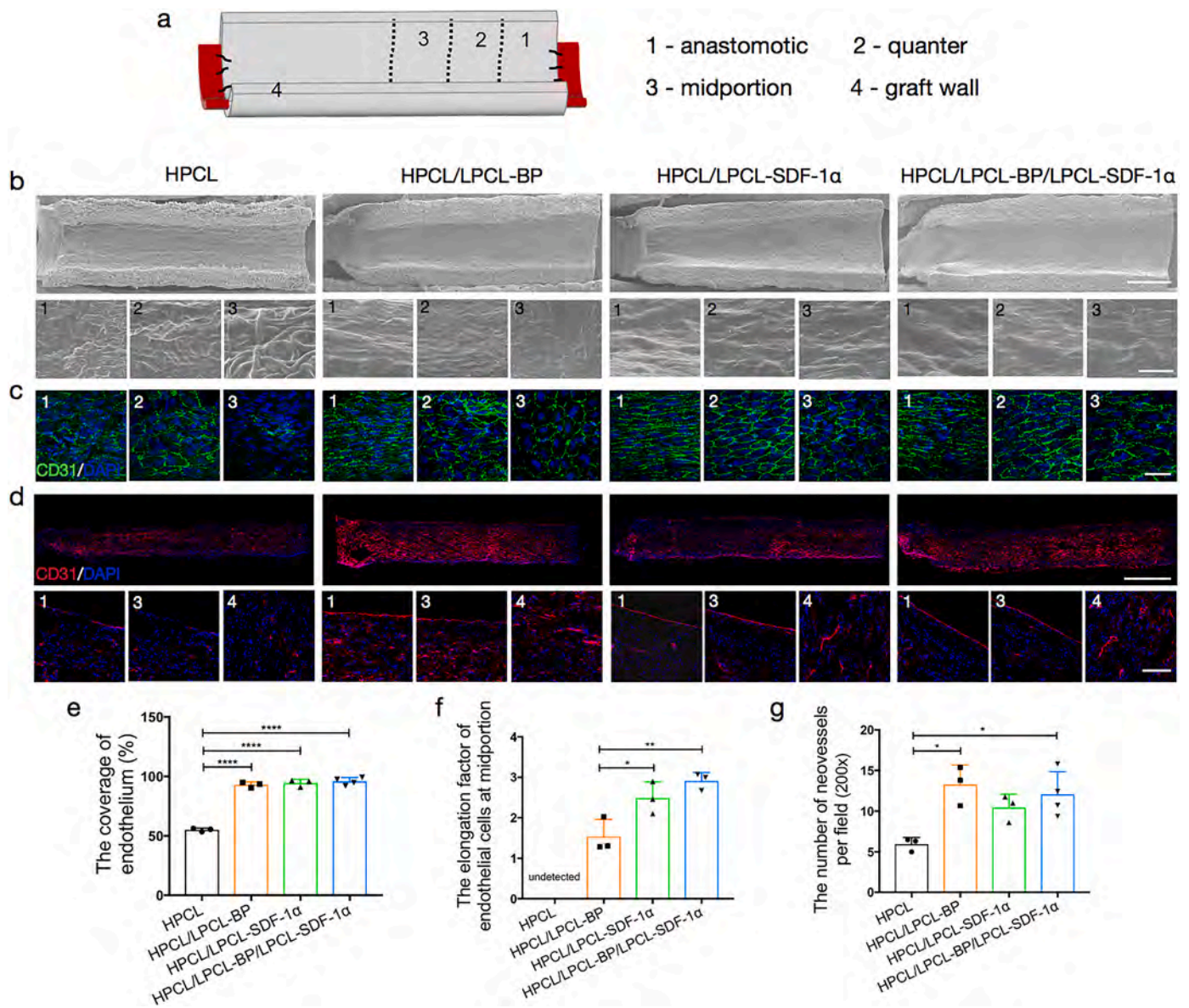


**Fig. 6.** Peptides modification enhances functional EC layer formation. (a) Schematic diagram of 4 sections of explanted vascular grafts. (b) SEM and (c) *enface* immunostaining images showed the morphology of luminal surface and ECs distribution at different sites (anastomotic - 1, quarter - 2, and midportion - 3). Scale bars for SEM images, 1 mm or 50  $\mu$ m (magnified images). Scale bars for *enface* immunostaining images, 50  $\mu$ m. (d) Immunofluorescence staining with CD31 antibody was performed on longitudinal sections of the explanted grafts (upper panel), and the lower panel showed the magnified images of different sites (anastomotic - 1, midportion - 3 and graft wall - 4). Scale bars, 1 mm or 100  $\mu$ m (magnified images). (e) The endothelium coverage rate was calculated by CD31 staining. (f) The elongation factor of ECs was calculated from *enface* staining at midportion part (c - 3). (g) The neovessels number in graft wall was calculated by CD31 staining (d - 4). \* $P < 0.05$ , \*\* $P < 0.01$ , \*\*\*\* $P < 0.0001$ .

short-term and long-term patency [45]. While the addition of LPCL-BP and LPCL-SDF-1 $\alpha$  to the HPCL grafts influenced the regeneration of vascular cell types, they showed similar patency to the HPCL grafts. The dual peptide-loaded grafts showed higher patency than that of single peptide-loaded grafts, which may be ascribed to the combined effect of BP and SDF-1 $\alpha$  peptides on improving vascular regeneration. While SDF-1 $\alpha$  peptide can mobilize and recruit endogenous cells, BP-mediated VEGF-binding may induce the differentiation of endogenously recruited cells into vascular cell types.

It is widely studied that cellular infiltration plays a pivotal role for cell-free tissue engineered vascular grafts. We quantified the total numbers of cells recruited into graft wall, the cell numbers were remarkably higher in HPCL/LPCL-BP and HPCL/LPCL-BP/LPCL-SDF-1 $\alpha$  vascular grafts (Fig. 5c and d). Since endogenous stem cells and progenitor cells, such as Sca-1 $^{+}$  VPCs can differentiate into ECs and SMCs,

they may contribute to the endothelialization and functional smooth muscle layer formation of vascular grafts [13,14]. Further evaluation of cellular components revealed significant recruitment of Sca-1 $^{+}$  VPCs in HPCL/LPCL-SDF-1 $\alpha$  and HPCL/LPCL-BP/LPCL-SDF-1 $\alpha$  grafts than that of HPCL and HPCL/LPCL-BP grafts (Fig. 5e and f). More importantly, these Sca-1 $^{+}$  VPCs were found to be further differentiated into CD31 $^{+}$  ECs and  $\alpha$ -SMA $^{+}$  SMCs (Fig. 5g-h).

The endothelium plays a vital role for the short-term and long-term performance of vascular grafts, which also confers hemocompatibility to vascular grafts. A series of strategies have been leveraged to promote endothelium formation, such as cell seeding, ECM coating, and bioactive modification [55-57]. The ECs may either migrate into grafts from adjacent vessels or from the surrounding tissues via the differentiation of the VPCs [14]. Besides, ECs may arise from the differentiation of the stem/progenitor cells from bone marrow (BM) or peripheral circulation

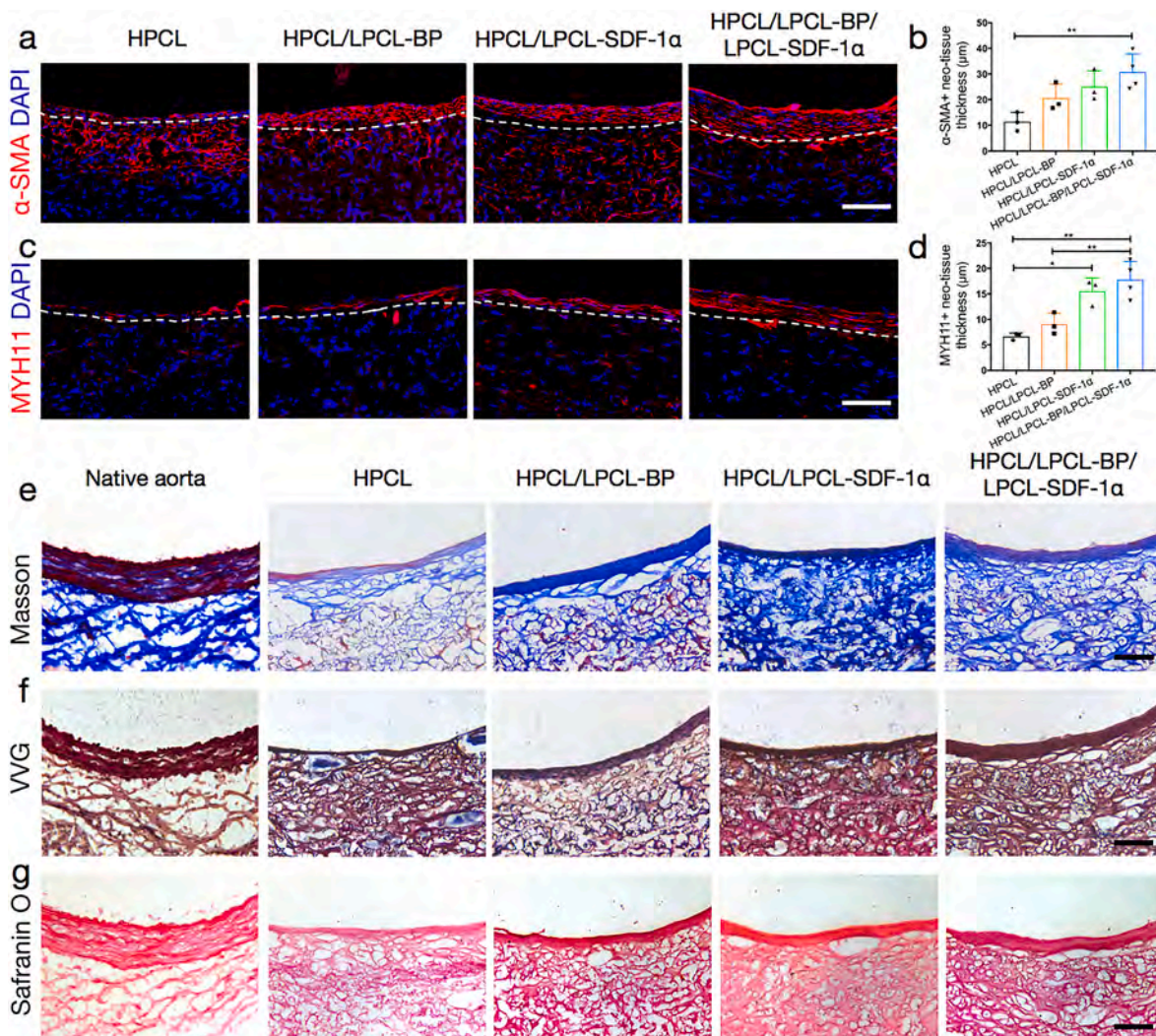


**Fig. 7.** Peptides modification improves vascular smooth muscle regeneration. (a) Representative immunofluorescence images showed SMCs regeneration by  $\alpha$ -SMA staining (white dashed lines indicate the luminal region). Scale bars, 100  $\mu$ m. (b) Quantification of the total area of  $\alpha$ -SMA positive cells in the luminal region. (c) Representative immunofluorescence images showed functional SMCs regeneration by MYH11 staining (white dashed lines indicate the luminal region). Scale bars, 100  $\mu$ m. (d) Quantification of the total area of MYH11 positive cells in the luminal region. (e–g) ECM deposition of vascular grafts was identified by Masson's Trichrome, VVG and Safranin O staining. Scale bars, 100  $\mu$ m \* $P$  < 0.05, \*\* $P$  < 0.01.

[58]. Both SEM analysis and immunofluorescence staining by using CD31 antibody revealed higher endothelium regeneration in bioactive grafts than that of the HPCL groups (Fig. 6b, d). *Enface* immunofluorescence staining by using CD31 showed regeneration of confluent ECs in bioactive grafts. Especially in the HPCL/LPCL-SDF-1 $\alpha$  and HPCL/LPCL-BP/LPCL-SDF-1 $\alpha$  grafts, ECs were organized along the direction of the blood flow and showed high elongation factor (Fig. 6c, f). The elongated ECs better mimic functional endothelium regeneration [6]. The BP can bind and stabilize VEGF, which is a potent angiogenic growth factor and may influence ECs adhesion and migration. Meanwhile, SDF-1 $\alpha$  can recruit VPCs as well as promote their differentiation into CD31 $^{+}$  ECs and  $\alpha$ -SMA $^{+}$  SMCs, and SMCs may also influence the ECs function, such as better organization and elongation [13]. Thus, the nice endothelialization in HPCL/LPCL-BP/LPCL-SDF-1 $\alpha$  grafts may be attributable to the combined effect of BP and SDF-1 $\alpha$  peptides.

In addition to endothelium regeneration, SMCs regeneration and ECM deposition have notable effects on neo-artery regeneration. The SMCs exhibit different phenotypes, including  $\alpha$ -SMA $^{+}$  synthetic phenotype and MYH11 $^{+}$  contractile phenotype; the latter plays a crucial role in the contraction/relaxation of blood vessels. Noticeably, HPCL/LPCL-SDF-1 $\alpha$  and HPCL/LPCL-BP/LPCL-SDF-1 $\alpha$  grafts also exhibited

significantly higher proportion of MYH11 $^{+}$  neo-tissues, which surrounded the endothelium (Fig. 7c and d). The bioactive grafts, especially, the HPCL/LPCL-BP/LPCL-SDF-1 $\alpha$  group also displayed native aorta mimetic regeneration of ECM components, including collagen, elastin, and GAGs in the graft wall than that of the HPCL grafts (Fig. 7e–g).

Biomaterial implantation also induces the infiltration of macrophages, which have been shown to exhibit different phenotypes, such as pro-inflammatory (M1) and anti-inflammatory (M2) phenotypes. Previously, a myriad of bioactive cues have been leveraged to promote vascular regeneration through immune-modulation. Roh et al. delineated higher patency of bone marrow mononuclear cells (BM-MNCs) loaded vascular grafts, which was mainly governed by the higher content of M2 macrophages [16]. The M2 type macrophages have been shown to partly contribute to the vascular repair via secreting different types of cytokines and chemokines, such as interleukin-4 (IL-4) and interleukin-10 (IL-10) [38,59]. The HPCL group consists of large pores, which exhibits anti-inflammatory response and drives macrophages polarization from M1 to M2 phenotypes [38]. The SDF-1 $\alpha$  peptide could polarize macrophages toward M2 phenotypes [19]. In this study, we observed significantly higher numbers of CD206 $^{+}$  macrophages as well

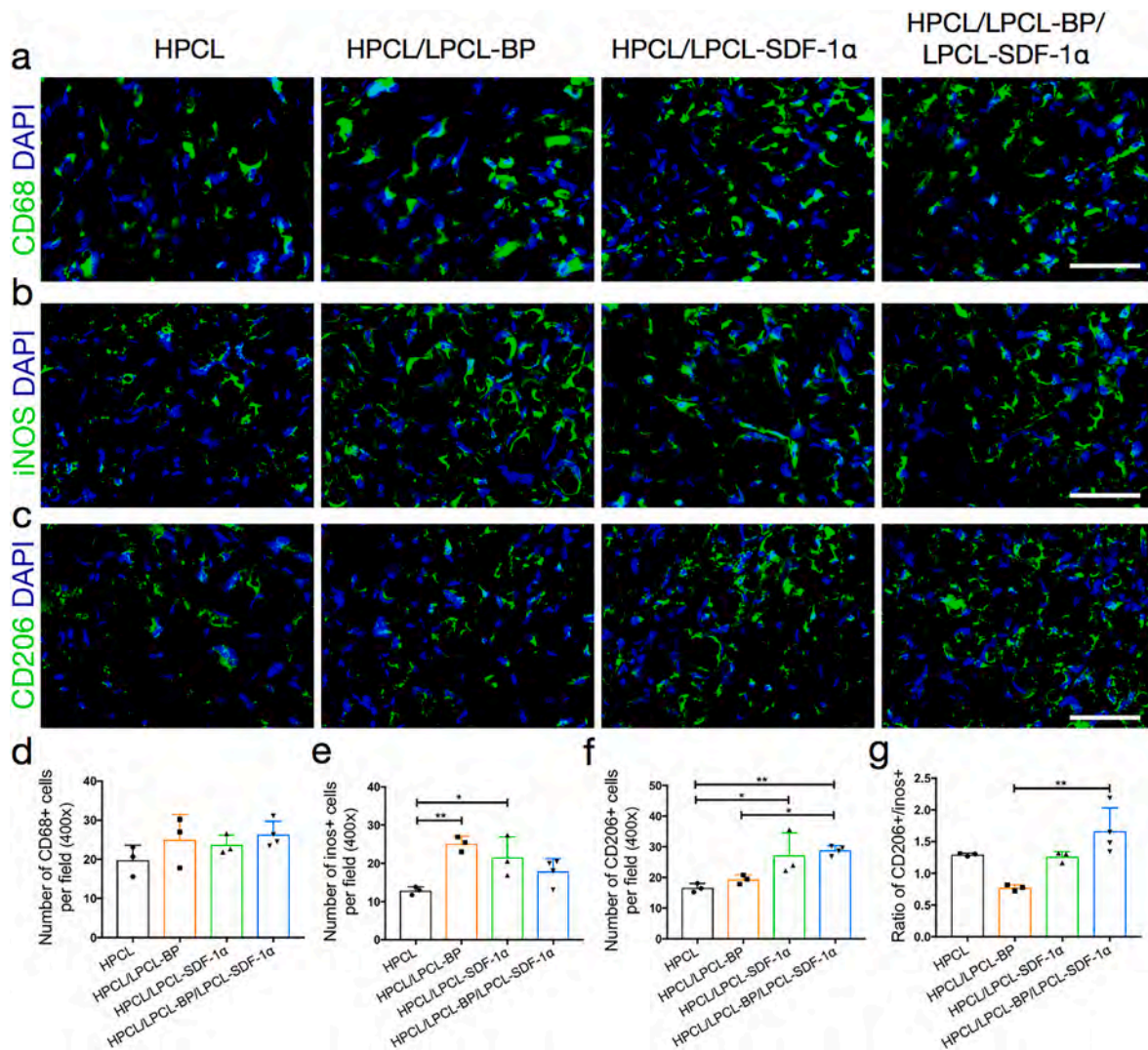


**Fig. 8.** Peptides modification promotes the polarization of macrophage to the M2 phenotype. (a–c) Representative immunofluorescence images exhibiting the infiltration of total, M1 and M2 macrophages by staining the cross-sections with anti-CD68, anti-iNOS and anti-CD206 antibodies, respectively. Scale bars, 50  $\mu$ m. (d–f) The number of the infiltrated total, M1 and M2 macrophages were quantified accordingly (400  $\times$  magnification). (g) The ratio of M2/M1 was quantified by CD206<sup>+</sup>/iNOS<sup>+</sup> cells. \* $P < 0.05$ , \*\* $P < 0.01$ .

as a higher ratio of CD206<sup>+</sup>/iNOS<sup>+</sup> macrophages in HPCL/LPCL-SDF-1 $\alpha$  group. Once the LPCL-BP was added to the graft, we observed higher inflammation than that of the HPCL grafts, which is indicated by the higher numbers of iNOS<sup>+</sup> macrophages. As BP can bind VEGF, the latter may enhance cellular infiltration into grafts. While compared to the HPCL group, HPCL/LPCL-BP showed more cells in the graft wall (Fig. 5d), which is also evident from the higher number of iNOS<sup>+</sup> macrophages. However, the BP did not show an immunomodulatory effect on macrophages polarization from M1 to M2 phenotype and the mechanism was unclear. In dual peptides loaded vascular grafts, it showed a higher ratio of CD206<sup>+</sup>/iNOS<sup>+</sup> macrophages, which is ascribed to the anti-inflammatory effect of SDF-1 $\alpha$  peptide (Fig. 8). Nonetheless, it requires further investigation if both peptides can act synergistically for immuno-modulation.

Our studies also have some limitations. We implanted grafts only for a short time-point. The long-term implantation of vascular grafts may further help elucidate their therapeutic effect. Similarly, we implanted grafts as abdominal aorta substitutes in rats. The implantation of grafts in other models, such as a rabbit, may further elucidate their potential for vascular grafting. The other bioactive molecules, such as heparin may be incorporated into vascular grafts to further confer them the hemocompatibility. Nonetheless, these bioactive vascular grafts

displayed higher endothelialization, vascular remodeling, and neo-artery regeneration.

## 5. Conclusion

In this study, we synthesized BP and SDF-1 $\alpha$  peptide conjugated LPCL and fabricated bioactive electrospun vascular grafts by blending the peptide-tethered LPCL with the HPCL. The BP and SDF-1 $\alpha$  peptides were co-leveraged to simultaneously harness VEGF-mediated endothelialization and neovascularization as well as SDF-1 $\alpha$ -induced endogenous stem/progenitor cell mobilization and recruitment. Chemical analysis revealed the successful conjugation of peptides with the LPCL as well as good cytocompatibility of scaffolds containing LPCL-BP and LPCL-SDF-1 $\alpha$ . The transplantation of vascular grafts as abdominal aorta substitutes revealed that the HPCL/LPCL-BP/LPCL-SDF-1 $\alpha$  group, which contained dual peptides, has significant effects on endothelialization, SMCs regeneration, endogenous cell recruitment, and inflammation resolution as compared to that of the HPCL grafts. Conclusively, bioactive vascular grafts amassed from dual peptide-tethered HPCL/LPCL-BP/LPCL-SDF-1 $\alpha$  may have broad implications for neo-artery regeneration as well as other related disciplines.

## Author statement

Yifan Wu: Project administration, Data curation, Funding acquisition, Writing - original draft; Lili Song: Software, Methodology, Data processing, Data curation; Muhammad Shafiq: Conceptualization, Data Curation, Methodology, Writing, Writing-Review &; Editing, Funding acquisition; Hiroyuki Ijima: Supervision, Funding acquisition; Soo Hyun Kim: Writing-Review &; Editing; Ran Wei: Software; Deling Kong: Supervision, Funding acquisition; Xiumei Mo: Supervision, Funding acquisition; Kai Wang: Supervision, Writing-Review &; Editing, Funding acquisition.

## Declaration of competing interest

The authors declare that they have no known competing financial interests or personal relationships that could have appeared to influence the work reported in this paper.

## Data availability

I have shared the link to my data/code at the Attach File step

## Acknowledgment

This work was supported by National Natural Science Foundation of China projects (No. 32101098, 32050410286), the Science & Technology Projects of Tianjin of China (No. 21JCQNJC01530) and China Postdoctoral Science Foundation (No. 2022M711704). The research was also supported by Science and Technology Commission of Shanghai Municipality (No. 20S31900900, 20DZ2254900), the outstanding project of the Chinese people's liberation army (PLA) Medical Science and Technology Youth Cultivation Program (18QNP059), Sino German Science Foundation Research Exchange Center (M – 0263) and the Grant-in-Aid for JSPS Research Fellows (Grant # JP21F21353). M.S is an International Research Fellow of the Japan Society for the Promotion of Science (JSPS) at the Department of Chemical Engineering, Kyushu University, Japan.

## Appendix A. Supplementary data

Supplementary data to this article can be found online at <https://doi.org/10.1016/j.compositesb.2023.110504>.

## References

- Arsalan M, Mack MJ. Coronary artery bypass grafting is currently underutilized. *Circulation* 2016;133(10):1036–45.
- Caliskan E, de Souza DR, Böning A, Liakopoulos OJ, Choi YH, Pepper J, Gibson CM, Perrault LP, Wolf RK, Kim KB, Emmert MY. Saphenous vein grafts in contemporary coronary artery bypass graft surgery. *Nature reviews. Cardiology* 2020;17(3):155–69.
- Kirkton RD, Santiago-Maysonet M, Lawson JH, Tente WE, Dahl SLM, Niklason LE, Prichard HL. Bioengineered human acellular vessels recellularize and evolve into living blood vessels after human implantation. *Sci Transl Med* 2019;11(485):eaau6934.
- Seifu DG, Purnama A, Mequanint K, Mantovani D. Small-diameter vascular tissue engineering. *Nat Rev Cardiol* 2013;10(7):410–21.
- Rafique M, Midgley AC, Wei T, Wang L, Kong D, Wang K. Controlling pore size of electrospun vascular grafts by electrospaying of poly(ethylene oxide) microparticles. *Methods Mol Biol* 2022;2375:153–64.
- Wang H, Xing M, Deng W, Qian M, Wang F, Wang K, Midgley AC, Zhao Q. Anti-Scal-1 antibody-functionalized vascular grafts improve vascular regeneration via selective capture of endogenous vascular stem/progenitor cells. *Bioact Mater* 2022;16:433–50.
- Wu W, Allen RA, Wang Y. Fast-degrading elastomer enables rapid remodeling of a cell-free synthetic graft into a neoartery. *Nat Med* 2012;18(7):1148–53.
- Zhu M, Wu Y, Li W, Dong X, Chang H, Wang K, Wu P, Zhang J, Fan G, Wang L, Liu J, Wang H, Kong D. Biodegradable and elastomeric vascular grafts enable vascular remodeling. *Biomaterials* 2018;183:306–18.
- Shafiq M, Wang L, Zhi D, Zhang Q, Wang K, Wang L, Kim DH, Kong D, Kim SH. In situ blood vessel regeneration using neuropeptide substance P-conjugated small-diameter vascular grafts. *J Biomed Mater Res B Appl Biomater* 2019;107(5):1669–83.
- Shafiq M, Kim SH. Biomaterials for host cell recruitment and stem cell fate modulation for tissue regeneration: focus on neuropeptide substance P. *Macromol Res* 2016;24(11):951–60.
- Zhu T, Gu H, Ma W, Zhang Q, Du J, Chen S, Wang L, Zhang W. A fabric reinforced small diameter tubular graft for rabbits' carotid artery defect. *Compos B Eng* 2021;225:109274.
- Sun Q, Si J, Zhao L, Wei T, Wang T, Li F, Li Y, Shafiq M, Wang L, Liu R, Zhi D, Wang K. Direct thrombin inhibitor-bivalirudin improved the hemocompatibility of electrospun polycaprolactone vascular grafts. *Compos B Eng* 2022;234:109702.
- Issa Bhaloo S, Wu Y, Le Bras A, Yu B, Gu W, Xie Y, Deng J, Wang Z, Zhang Z, Kong D, Hu Y, Qu A, Zhao Q, Xu Q. Binding of dickkopf-3 to CXCR7 enhances vascular progenitor cell migration and degradable graft regeneration. *Circ Res* 2018;123(4):451–66.
- Pan Y, Yang J, Wei Y, Wang H, Jiao R, Moraga A, Zhang Z, Hu Y, Kong D, Xu Q, Zeng L, Zhao Q. Histone deacetylase 7-derived peptides play a vital role in vascular repair and regeneration. *Adv Sci* 2018;5(8):1800006.
- Best C, Tara S, Wiet M, Reinhardt J, Pepper V, Ball M, Yi T, Shinoka T, Breuer C. Deconstructing the tissue engineered vascular graft: evaluating scaffold pre-wetting, conditioned media incubation, and determining the optimal mononuclear cell source. *ACS Biomater Sci Eng* 2017;3(9):1972–9.
- Roh JD, Sawh-Martinez R, Brennan MP, Jay SM, Devine L, Rao DA, Yi T, Mirensky TL, Nalbandian A, Udelsman B, Hibino N, Shinoka T, Saltzman WM, Snyder E, Kyriakides TR, Pober JS, Breuer CK. Tissue-engineered vascular grafts transform into mature blood vessels via an inflammation-mediated process of vascular remodeling. *Proc. Natl. Acad. Sci. U.S.A* 2010;107(10):4669–74.
- Fayon A, Menu P, El Omar R. Cellularized small-caliber tissue-engineered vascular grafts: looking for the ultimate gold standard. *NPJ Regen. Med.* 2021;6(1):46.
- Shafiq M, Jung Y, Kim SH. In situ vascular regeneration using substance P-immobilised poly(L-lactide-co-ε-caprolactone) scaffolds: stem cell recruitment, angiogenesis, and tissue regeneration. *Eur Cell Mater* 2015;30:282–302.
- Shafiq M, Zhang Q, Zhi D, Wang K, Kong D, Kim DH, Kim SH. In situ blood vessel regeneration using SP (substance P) and SDF (stromal cell-derived factor)-1α peptide eluting vascular grafts. *Arterioscler Thromb Vasc Biol* 2018;38(7):e117–34.
- Antonova LV, Sevostyanova VV, Kutikhin AG, Mironov AV, Krivkina EO, Shabaev AR, Matveeva VG, Velikanova EA, Sergeeva EA, Burago AY, Vasyukov GY, Glushkova TV, Kudryavtseva YA, Barbarash OL, Barbarash LS. Vascular endothelial growth factor improves physico-mechanical properties and enhances endothelialization of poly(3-hydroxybutyrate-co-3-hydroxyvalerate)/poly(ε-caprolactone) small-diameter vascular grafts in vivo. *Front Pharmacol* 2016;7:230.
- Lee SJ, Kim ME, Nah H, Seok JM, Jeong MH, Park K, Kwon IK, Lee JS, Park SA. Vascular endothelial growth factor immobilized on mussel-inspired three-dimensional bilayered scaffold for artificial vascular graft application: in vitro and in vivo evaluations. *J Colloid Interface Sci* 2019;537:333–44.
- Antonova L, Kutikhin A, Sevostianova V, Velikanova E, Matveeva V, Glushkova T, Mironov A, Krivkina E, Shabaev A, Senokosova E, Barbarash L. bFGF and SDF-1α improve in vivo performance of VEGF-incorporating small-diameter vascular grafts. *Pharmaceuticals* 2021;14(4):302.
- Chi ZL, Adini A, Birsner AE, Bazinet L, Akula JD, D'Amato RJ. PR1P ameliorates neurodegeneration through activation of VEGF signaling pathway and remodeling of the extracellular environment. *Neuropharmacology* 2019;148:96–106.
- Yuan Z, Sheng D, Jiang L, Shafiq M, Khan AUR, Hashim R, Chen Y, Li B, Xie X, Chen J, Morsi Y, Mo X, Chen S. Vascular endothelial growth factor-capturing aligned electrospun polycaprolactone/gelatin nanofibers promote patellar ligament regeneration. *Acta Biomater* 2022;140:233–46.
- Adini A, Wu H, Dao DT, Ko VH, Yu LJ, Pan A, Puder M, Mitiku SZ, Potla R, Chen H, Rice JM, Matthews BD. PR1P stabilizes VEGF and upregulates its signaling to reduce elastase-induced murine emphysema. *Am J Respir Cell Mol Biol* 2020;63(4):452–63.
- Adini A, Adini I, Chi ZL, Derda R, Birsner AE, Matthews BD, D'Amato RJ. A novel strategy to enhance angiogenesis in vivo using the small VEGF-binding peptide PR1P. *Angiogenesis* 2017;20(3):399–408.
- Smith Jr RJ, Nasiri B, Kann J, Yergeau D, Bard JE, Swartz DD, Andreadis ST. Endothelialization of arterial vascular grafts by circulating monocytes. *Nat Commun* 2020;11(1):1622.
- Shafiq M, Ali O, Han SB, Kim DH. Mechanobiological strategies to enhance stem cell functionality for regenerative medicine and tissue engineering. *Front Cell Dev Biol* 2021;9:747398.
- Schumacher M, Habibovic P, van Rijt S. Peptide-modified nano-bioactive glass for targeted immobilization of native VEGF. *ACS Appl Mater Interfaces* 2022;14(4):4959–68.
- Yu J, Wang A, Tang Z, Henry J, Li-Ping Lee B, Zhu Y, Yuan F, Huang F, Li S. The effect of stromal cell-derived factor-1α/heparin coating of biodegradable vascular grafts on the recruitment of both endothelial and smooth muscle progenitor cells for accelerated regeneration. *Biomaterials* 2012;33(32):8062–74.
- Segers VF, Tokunou T, Higgins LJ, MacGillivray C, Gannon J, Lee RT. Local delivery of protease-resistant stromal cell derived factor-1 for stem cell recruitment after myocardial infarction. *Circulation* 2007;116(15):1683–92.
- Shafiq M, Kong D, Kim SH. SDF-1α peptide tethered polyester facilitates tissue repair by endogenous cell mobilization and recruitment. *J Biomed Mater Res, Part A* 2017;105(10):2670–84.
- Muylaert DE, van Almen GC, Talacua H, Fledderus JO, Kluijn J, Hendrikse SI, van Dongen JL, Sijbesma E, Bosman AW, Mes T, Thakkar SH, Smits AI, Bouten CV,

- Dankers PY, Verhaar MC. Early in-situ cellularization of a supramolecular vascular graft is modified by synthetic stromal cell-derived factor-1 $\alpha$  derived peptides. *Biomaterials* 2016;76:187–95.
- [34] Sun XY, Shankar R, Borner HG, Ghosh TK, Spontak RJ. Field-driven biofunctionalization of polymer fiber surfaces during electrospinning. *Adv Mater* 2007;19(1):87.
- [35] Gentsch R, Pippig F, Schmidt S, Cernoch P, Polleux J, Borner HG. Single-step electrospinning to bioactive polymer nanofibers. *Macromolecules* 2011;44(3):453–61.
- [36] Camacho P, Busari H, Seims KB, Schwarzenberg P, Dailey HL, Chow LW. 3D printing with peptide-polymer conjugates for single-step fabrication of spatially functionalized scaffolds. *Biomater Sci* 2019;7(10):4237–47.
- [37] Chow LW, Armgarth A, St-Pierre JP, Bertazzo S, Gentilini C, Aurisicchio C, McCullen SD, Steele JA, Stevens MM. Peptide-directed spatial organization of biomolecules in dynamic gradient scaffolds. *Adv. Healthc. Mater.* 2014;3(9):1381–6.
- [38] Wang Z, Cui Y, Wang J, Yang X, Wu Y, Wang K, Gao X, Li D, Li Y, Zheng XL, Zhu Y, Kong D, Zhao Q. The effect of thick fibers and large pores of electrospun poly( $\epsilon$ -caprolactone) vascular grafts on macrophage polarization and arterial regeneration. *Biomaterials* 2014;35(22):5700–10.
- [39] Rafique M, Wei T, Sun Q, Midgley AC, Huang Z, Wang T, Shafiq M, Zhi D, Si J, Yan H, Kong D, Wang K. The effect of hypoxia-mimicking responses on improving the regeneration of artificial vascular grafts. *Biomaterials* 2021;271:120746.
- [40] Zhu J, Chen D, Du J, Chen X, Wang J, Zhang H, Chen S, Wu J, Zhu T, Mo X. Mechanical matching nanofibrous vascular scaffold with effective anticoagulation for vascular tissue engineering. *Compos B Eng* 2020;186:107788.
- [41] Zhu M, Wang Z, Zhang J, Wang L, Yang X, Chen J, Fan G, Ji S, Xing C, Wang K, Zhao Q, Zhu Y, Kong D, Wang L. Circumferentially aligned fibers guided functional neovessel regeneration in vivo. *Biomaterials* 2015;61:85–94.
- [42] Rhee J, Shafiq M, Kim D, Jung Y, Kim SH. Covalent immobilization of EPCs-affinity peptide on Poly(L-Lactide-co- $\epsilon$ -Caprolactone) copolymers to enhance EPCs adhesion and retention for tissue engineering applications. *Macromol Res* 2018;27:61–72.
- [43] Shin YC, Kim J, Kim SE, Song SJ, Hong SW, Oh JW, Lee J, Park JC, Hyon SH, Han DW. RGD peptide and graphene oxide co-functionalized PLGA nanofiber scaffolds for vascular tissue engineering. *Regen. Biomater.* 2017;4(3):159–66.
- [44] Al-Dhahebi AM, Ling J, Krishnan SG, Yousefzadeh M, Elumalai NK, Saheed MSM, Ramakrishna S, Jose R. Electrospinning research and products: the road and the way forward. *Appl Phys Rev* 2022;9(1):011319.
- [45] Wu Y, Qin Y, Wang Z, Wang J, Zhang C, Li C, Kong D. The regeneration of macro-porous electrospun poly( $\epsilon$ -caprolactone) vascular graft during long-term in situ implantation. *J Biomed Mater Res B Appl Biomater* 2018;106(4):1618–27.
- [46] Dai C, Chu T, Li X, Jiang H, Liu T, Zhou Y, Gao L, Shen C, Ge J. A novel UV-curable extravascular stent to prevent restenosis of venous grafts. *Compos B Eng* 2021;225:109260.
- [47] Wei Y, Wu Y, Zhao R, Zhang K, Midgley AC, Kong D, Li Z, Zhao Q. MSC-derived sEVs enhance patency and inhibit calcification of synthetic vascular grafts by immunomodulation in a rat model of hyperlipidemia. *Biomaterials* 2019;204:13–24.
- [48] Wang Z, Zheng W, Wu Y, Wang J, Zhang X, Wang K, Zhao Q, Kong D, Ke T, Li C. Differences in the performance of PCL-based vascular grafts as abdominal aorta substitutes in healthy and diabetic rats. *Biomater Sci* 2016;4(10):1485–92.
- [49] Wen M, Zhi D, Wang L, Cui C, Huang Z, Zhao Y, Wang K, Kong D, Yuan X. Local delivery of dual MicroRNAs in trilayered electrospun grafts for vascular regeneration. *ACS Appl Mater Interfaces* 2020;12(6):6863–75.
- [50] Jun HW, West JL. Endothelialization of microporous YIGSR/PEG-modified polyurethaneurea. *Tissue Eng* 2005;11(7–8):1133–40.
- [51] Liang Q, Gao F, Zeng Z, Yang J, Wu M, Gao C, Cheng D, Pan H, Liu W, Ruan C. Coaxial scale-up printing of diameter-tunable biohybrid hydrogel microtubes with high strength, Perfusability, and Endothelialization. *Adv. Funct. Mater.* 2020;30(43):2001485.
- [52] Wu P, Wang L, Li W, Zhang Y, Wu Y, Zhi D, Wang H, Wang L, Kong D, Zhu M. Construction of vascular graft with circumferentially oriented microchannels for improving artery regeneration. *Biomaterials* 2020;242:119922.
- [53] Zhu M, Li W, Dong X, Yuan X, Midgley AC, Chang H, Wang Y, Wang H, Wang K, Ma PX, Wang H, Kong D. In vivo engineered extracellular matrix scaffolds with instructive niches for oriented tissue regeneration. *Nat Commun* 2019;10(1):4620.
- [54] Jin Q, Fu Y, Zhang G, Xu L, Jin G, Tang L, Ju J, Zhao W, Hou R. Nanofiber electrospinning combined with rotary bioprinting for fabricating small-diameter vessels with endothelium and smooth muscle. *Compos B Eng* 2022;234:109691.
- [55] Wang Z, Lu Y, Qin K, Wu Y, Tian Y, Wang J, Zhang J, Hou J, Cui Y, Wang K, Shen J, Xu Q, Kong D, Zhao Q. Enzyme-functionalized vascular grafts catalyze in-situ release of nitric oxide from exogenous NO prodrug. *J Contr Release : Off. J. Control. Release Soc.* 2015;210:179–88.
- [56] Pasic M, Müller-Glauser W, von Segesser L, Odermatt B, Lachat M, Turina M. Endothelial cell seeding improves patency of synthetic vascular grafts: manual versus automatized method. *Eur J Cardio Thorac Surg : Off. J. Eur. Assoc. Cardio-thoracic Surg.* 1996;10(5):372–9.
- [57] Wang F, Qin K, Wang K, Wang H, Liu Q, Qian M, Chen S, Sun Y, Hou J, Wei Y, Hu Y, Li Z, Xu Q, Zhao Q. Nitric oxide improves regeneration and prevents calcification in bio-hybrid vascular grafts via regulation of vascular stem/progenitor cells. *Cell Rep* 2022;39(12):110981.
- [58] Talacua H, Smits AI, Muylaert DE, van Rijswijk JW, Vink A, Verhaar MC, Driessen-Mol A, van Herwerden LA, Bouten CV, Kluin J, Baaijens FP. In situ tissue engineering of functional small-diameter blood vessels by host circulating cells only, tissue engineering. *Part Accel* 2015;21(19–20):2583–94.
- [59] Hibino N, Mejias D, Pietris N, Dean E, Yi T, Best C, Shinoka T, Breuer C. The innate immune system contributes to tissue-engineered vascular graft performance. *Faseb J : Off. Publ. Federation. Am. Soc. Exp. Biol.* 2015;29(6):2431–8.